AD-A014 619

DEVELOPMENT OF TECHNOLOGY FOR ASSESSMENT OF ELECTROMAGNETIC COUPLING - AUTOMATION AND EXTENSION OF MIL-STD-1377

McDonnell Douglas Astronautics Company - East

Prepared for:

Naval Surface Weapons Center

28 February 1975

DEVELOPMENT OF TECHNOLOGY FOR ASSESSMENT OF ELECTROMAGNETIC COUPLING

AUTOMATION AND EXTENSION OF MIL-STD-1377

MCDONNELL DOUGLAS ASTRONAUTICS COMPANY - EAST

MCDONNELL DOUGLAS
CORPORATION

COPY NO. 39

DEVELOPMENT OF TECHNOLOGY FOR ASSESSMENT OF ELECTROMAGNETIC COUPLING

MDC E1225 28 FEBRUARY 1975

AUTOMATION AND EXTENSION OF MIL-STD-1377

SUBMITTED TO:
NAVAL SURFACE WEAPONS CENTER – DAHLGREN LABORATORY
DAHLGREN, VA 22448
CONTRACT NO. N00178-74-C-0524

MCDONNELL DOUGLAS ASTRONAUTICS COMPANY - EAST
Saint Louis, Missouri 63166 (314) 232-0232

MCDONNELL DOUGLAS CORPORATION

Table of Contents

List of Pages

Title Page

i

1 through 71

1. Introduction and Summary

This document is the second of two reports prepared under contract N00178-74-C-0524, Development of Technology for Assessment of Electromagnetic Coupling. The subject of the first report (MDC Report E1178) was the shielding effectiveness of aerospace enclosures (designated as Task I); this report deals with improvements in the techniques for measuring shielding effectiveness (Task II).

1.1 Introduction - Electromagnetic energy can be coupled from radiation fields to electronic system wiring and, depending upon the connections of the wiring, electromagnetic interference (EMI) can result in the system. The thrust of this contract is to develop a better understanding of the coupling mechanisms, and to improve the technology for assessing electromagnetic coupling in the one to ten gigahertz frequency range.

The essence of the approach is to consider system wiring as receiving antennas which can be characterized in terms of an effective aperture, and to determine the effectiveness of various shielding techniques (including inherent shielding provided by system skin, etc.) for reducing the amount of energy coupled onto the wiring. The "real world" standard of comparison is the amount of energy picked up on test samples (shielded and unshielded) in an anechoic chamber measurement. Since anechoic chamber measurements are time-consuming and costly, an improved method for assessing coupling is highly desirable.

There are different techniques for measuring shielding effectiveness (the relative reduction of coupling), but MIL-STD-1377 (Navy) has been found to be the most reliable in terms of repeatibility and the ability to determine the minimum degree of shielding available. The MIL-STD-1377 technique is also relatively simple and rapid. The work discussed in the first report of this series (MDC Report E1178) was designed to determine the possible correlation between MIL-STD-1377 measurements of typical aerospace enclosures and anechoic chamber measurements of the coupled

power levels. Nineteen complete test cases were measured in the anechoic chamber (including variations of test sample configuration and frequency) for comparison to a series of eight MIL-STD-1377 measurements made in the laboratory. It was demonstrated that the pick up power can be treated as a random variable which depends upon the aspect angle of the test specimen to the emitter and (for enclosure samples) the internal configuration of the pick up wire and the enclosure. A strict application of MIL-STD-1377 results will predict only the worst-case (i.e., highest degree) of coupling levels. Actual coupling into a given system with a particular internal wiring configuration may be lower than this by as much as 40dB. By utilizing an expanded view of the MIL-STD-1377 concept, a statistical interpretation of data resulting from internal and external tuning as described herein may permit estimates of the most probable pickup levels. Application of this new approach requires large amounts of data which are best handled by a computer. This fact provides the impetus for the work described in this report to automate the MIL-STD-1377 measurement technique.

1.2 Summary - In accomplishing Task II, a new scheme for tuning the MIL-STD-1377 chamber was invented which reduced the number of tuning variables from six to two. The efficiency of the new tuning scheme was demonstrated by comparing it to the MIL-STD-1377 technique for 28 complete shielding effectiveness measurements over the 1-10 GHz frequency range. This work clearly shows the feasibility of placing the shielding effectiveness measurement under computer control, and a simple demonstration of swept frequency data collection shows that the required amounts of data can be quickly collected. Further refinements in the data collection technique, however, are required.

A "calibration factor" was obtained relating injected power into the TEMEC chamber to the power densities used in anechoic chamber tests. Proof of its generality with respect to other test samples will require more anechoic chamber data for comparison.

2. Automation and Extension of the MIL-STD-1377 Technique

Task II was to determine the feasibility of automating the MIL-STD-1377 measurement technique, and determine the relationship between input power, maximum power density, and statistical distribution of power picked up by the test specimen in the TEMEC test chamber. A new scheme for tuning the MIL-STD-1377 chamber was invented, and it was shown that automating the procedure is feasible. The relationships among input power to the TEMEC chamber, maximum power density in the chamber, and the statistical distribution of power picked up by the test specimen were measured and the concept of an absolute TEMEC calibration appears feasible, but more anechoic chamber data are required to reduce the uncertainties in the calibration factor.

2.1 Background Description of MIL-STD-1377 - The basic idea of the MIL-STD-1377 shielding effectiveness measurement is to place the test specimen inside a specially constructed test chamber with provisions for injecting an electromagnetic signal while monitoring the amount of power picked up on the test specimen. Efforts are then made to maximize the power coupled onto the test specimen by adjusting various tuning devices. The theory is that if one finds the maximum amount of power that can be transferred to the test cable, one can infer that the difference between it and a reference cable is intrinsic to the test specimen and is its shielding effectiveness. Figure 1 shows schematically the MIL-STD-1377 test chamber and tuning devices. Standard coaxial lines are used for input and output with stub tuners to control the impedance at the two ports. Inside the chamber, paddle wheel tuners, consisting of dipoles which can be rotated and moved laterally provide for adjustment of the internal fields. When cable shielding effectiveness tests are being run, only one dipole tuner is needed; enclosure tests require a second dipole tuner located inside the enclosure under test. To minimize the losses and other

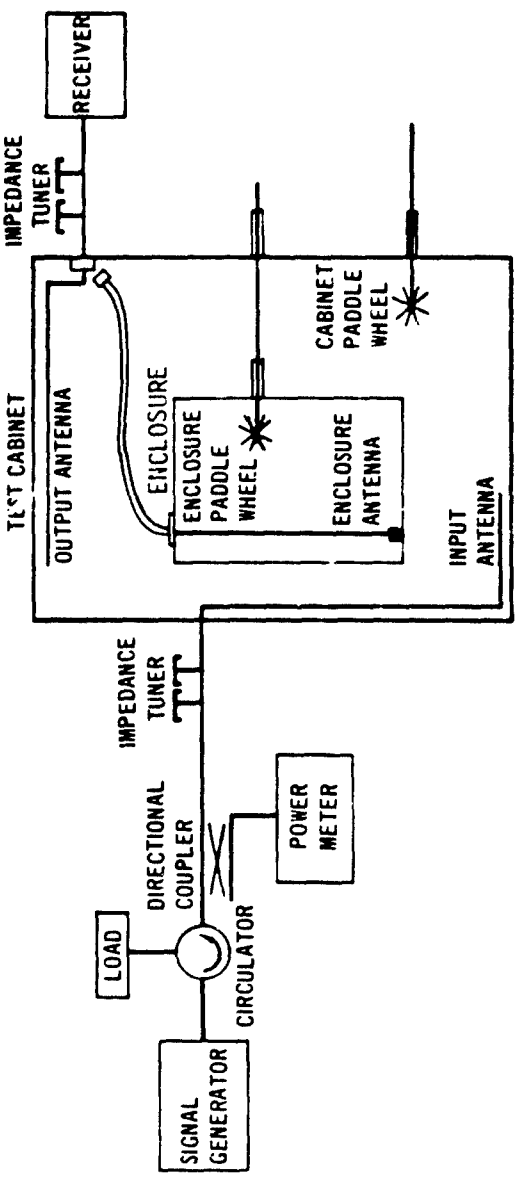

Figure 1 MIL-STD-1377 TEST SET-UP

undesirable effects, the dipoles are mounted on dielectric rods which pass through the chamber walls via waveguide below-cutoff tubes. In practice, the cabinet losses (as measured between the injection antenna and a reference pickup antenna) can be quite small over a usable frequency range of 1 to 10 GHz.

In operation, the test specimen is placed inside the chamber, a microwave signal of the desired frequency is injected into the chamber, and the operator manually adjusts the various tuning devices in a somewhat iterative manner to find the maximum power that can be coupled through the test specimen. Along the way, many local maxima are observed in which a tuning position is found for which any further tuning reduces the power transfer. By investigating a number of these local maxima, the operator finds the largest observable in a reasonable amount of time and it is assumed that this value (shield loss) is indicative of the intrinsic shielding effectiveness of the specimen. Comparison of this result to that obtained by looking at the unshielded reference antenna (calibration measurement) inside the chamber yields the shielding effectiveness value for the test specimen. The strength of this procedure is that it is highly repeatable with different operators and reconstructions of the experiments. The ability to find the absolute maximum tuning condition undoubtedly depends, to some degree, on the test chamber parameters, tuning system design, and operator skill, but results obtained have been very satisfactory compared to previous shielding effectiveness techniques.

The ability to automate this procedure depend upon finding some combination of simplified tuning and emulation of human judgement, or use of the sheer measurement power of a computer to randomly locate the maximum tuning condition (simplified tuning would result in greater efficiency here as well). As will be shown below, we were able to invent a new tuning scheme which reduces the number of tuning variables from six to two so that implementation of the random tuning concept is now quite viable.

2.2 Automation - As mentioned above, our efforts to automate the MIL-STD-1377 technique centered upon the simplification of the tuning scheme. To this end we invented a paddle wheel tuner requiring only rotation, and showed that the external stub tuners (both input and output) can be eliminated without significant degradation in measurement accuracy.

2.2.1 Paddle Wheel Tuners - The chief problem with the dipole tuners is the need for lateral movement (i.e., in and out motion) to provide sufficient tuning capability. Not only does the lateral motion increase the time required for an optimum adjustment but the mechanization of this motion under computer control is far more complex than for simple rotational devices (e.g., motors). To eliminate the need for linear motion, we developed a paddle wheel tuner with three dimensional properties somewhat resembling fan blades (hence, are designated as fan tuners) as shown in figure 2. The radius and pitch are selected to be approximately one half wavelength at the lowest frequency of interest. The fan is still attached to a dielectric rod for positioning and control (now consisting only of rotation).

To evaluate this design, the fan tuner replaced the dipole tuner in the MIL-STD-1377 chamber and a new series of shielding effectiveness measurements were run on the test samples described in MDC Report E1178 under Task I. Briefly these test samples consisted of a bare wire, a twisted-shielded cable, a section of RG-8/U cable, and five enclosures (4-inch diameter aluminum cylinders with various discontinuities). Table 1 tabulates the relative differences between the two sets of measurements. Note that positive values in this table imply that the fan tuner produced higher power transfers than did the dipole tuner, thereby implying greater tuning efficiency. The large improvements occurred in the enclosure measurements which used two fan tuners. The fan used inside the test specimen had to be smaller than the chamber fan to fit the small specimens. See figure 3.

Figure 2 **FAN TUNER**

TWIST 45° TO GIVE 8" LENGTH AT OUTSIDE EDGE ON TWO PROJECTED VIEWS IN PLANES 90° FROM EACH OTHER.

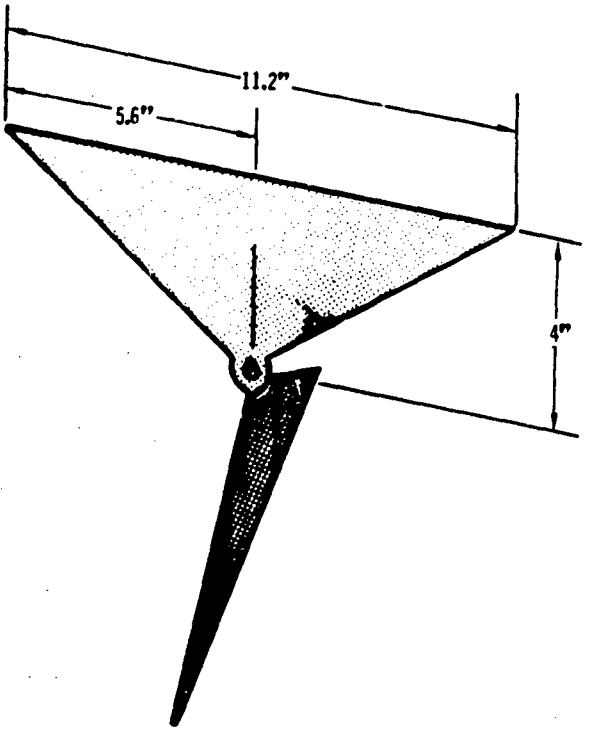

Table 1 Fan Tuner Improvement

Difference* Between Measurement Using Dipole Tuner and Fan Tuner

Freq.	Bare Wire	Twisted Shielded Pair	RG-8/U	Enclosure #1	Enclosure #2	Enclosure #3	Enclosure #4	Enclosure #5
1 GHz	0 dB	-2 dB	0 dB	- dB	- dB	- dB	- dB	-2.5 dB
1.5	0	-1	+1	-	+6	+8.5	-	-8
2	-1	+1	+1	-4	+5.5	-21.5	-5.5	0
2.5	0	0	-3	+9	-4	0	+18	+1
3	+1	+1	-1	+10	-9	+2	0	-6.5
3.5	0	-2	+2	+6	+19	+4	+11	+7
4	+1	-4	-2	+11	+3	+6	+4.5	+13
4.5	0	-0.5	-2	+1	+4	+5	+5	-3
5	0	+1	+2	+16	+17	+5	+6	+4.5
5.6	-1	0	-1	0	+5	+6.5	+5	+8.5
6	0	-0.5	-1	+5	+6	+9	+2.5	-2
6.5	0	-3	-1	+10	+10	-5	-3	+2
7	0	-1	0	+12.5	+4	+7	+5	+4
7.5	0	0	-1	+8.5	+13	+12.5	+4.5	+1.5
8	+2	+2	0	+6.5	+8	+1.5	+2	+2
8.5	0	-1	+1	+6.5	+3	+4	-2	-3
9.1	+2	-1	-2	+6	+15.5	+6	+2	+4.5
9.5	0	+1	0	+13	+9	+17	+2.5	+3
10.	+1	-2	-1	+6.5	+10.5	+9	-1	-2.5
Minimum	-1	-4	-3	-4	-9	-21.5	-5.5	-8
Maximum	+2	+2	+2	+16	+19	+17	+18	+13
Average	0.26	-0.63	-0.42	7.2	7.0	4.25	3.3	1.2

* See Figure A-1 Through A-9 For Specific Data

Figure 3 ENCLOSURE FAN TUNER

TWIST TOP VANE BACK 45° AND BOTTOM VANE FORWARD 45°

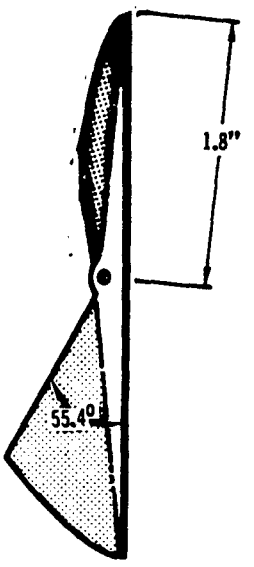

Our conclusion is that the new fan tuners can successfully replace the old dipole tuners in the MIL-STD-1377 test setup with resulting increase in tuning efficiency and decrease in complexity.

2.2.2 Tuner Effectiveness - The second part of our tuning simplification effort considered the relative effectiveness of the different tuners by determining what adverse effects, if any, resulted from elimination of each tuner in sequence.

2.2.2.1 Output Impedance Tuner - Since operating experience had shown that the stub tuner on the output of the chamber (between the test specimen and the receiver) was rarely used, we decided to study it first. The procedure was simply to remove it from the test setup and measure the shielding effectiveness of the test specimens as described above (except the RG-8/U). Comparison of the results to the full tuner set results provides a measure of its necessity.

Table 2 tabulates the differences between the shielding effectiveness measurements made by not using the output tuner and those made with the full set. Once again positive values imply improvements in tuning efficiency. In this case it can be seen that the differences are generally negligible, with the possible exception of the twisted-shielded cable measurement. In general, however, we believe the efficiency of the output tuner is low enough to safely omit it for most measurements.

2.2.2.2 Input Impedance Tuner - To test the efficiency and contribution of the input stub tuner, the same experiment as above was repeated by omitting the input tuner and making a full series of shielding effectiveness measurements. Table 3 presents the differences between these measurements and the reference data taken with all tuners. Again the differences are seen to be negligible.

2.2.2.3 Both Impedance Tuners - The results discussed above indicate one or the other stub tuner can be eliminated, but it is necessary to verify that both can be omitted. Accordingly, a full set of shielding effectiveness measurements

Table 2 Effect of Output Impedance Tuner

Difference* Between Not Using Output Tuner and Using All Tuners

Freq.	Calibration Loss	Twisted Shielded Pair	Enclosure #1	Enclosure #2	Enclosure #3	Enclosure #4	Enclosure #5
1 GHz	-1 dB	-1 dB	-2dB	0 dB	- dB	-3 dB	-2 dB
1.5	-	-3	-	-	-	-2	+7
2	+1	-3	+1	+1	-2	-1	-1
2.5	-2	-5	0	+1	0	-3	-2
3	-2	-7	-2	+1	0	0	0
3.5	-1	-5	+2	-2	0	+1	0
4	0	-6	-2	-1	-1	0	+1
4.5	0	-9	-2	-5	0	0	+2
5	-1	-6	-7	-1	+1	-1	-2
5.6	+1	-5	0	0	-1	+1	+1
6	0	-7	0	-1	0	+1	0
6.5	+1	-7	-3	-2	+3	-6	0
7	0	-10	-2	+2	-3	0	0
7.5	0	-9	0	-2	0	+1	0
8	+4	-10	+1	-1	0	+4	+1
8.5	0	-5	-2	+1	+5	-1	0
9.1	0	-5	+2	0	0	0	-2
9.5	+2	-2	+2	+2	-1	0	-1
10	0	-2	-1	0	0	+4	0
Maximum	+4	-1	+2	+2	+5	+6	+7
Minimum	-2	-10	-7	-5	-3	-3	-2
Average	+0.11	-5.6	-0.83	-0.39	+0.058	+0.037	0.11

* See Figures A-10 through A-16 For Specific Data

Table 3 Effect of Input Impedance Tuner

Difference* Between Not Using Input Tuner and Using All Tuners

Freq	Calibration Loss	Twisted Shielded Pair	Enclosure #1	Enclosure #2	Enclosure #3	Enclosure #4	Enclosure #5
1 GHz	0 dB	+5 dB	0 dB	-1 dB	- dB	+2 dB	-1 dB
1.5	-	+1	-	0	-3	-6	-4
2	+2	-1	-3	+1	-2	-1	-3
2.5	-2	-1	-2	+2	-1	-1	+1
3	-1	-1	-3	+6	-1	-2	-4
3.5	-3	-2	+1	0	0	-2	-1
4	+2	-1	-1	0	-2	+1	+1
4.5	-3	0	-2	-2	0	+1	+2
5	-1	+1	-6	-1	0	-2	+2
5.6	+2	-1	+3	0	+2	+1	-1
6	+2	+2	0	+3	+3	+1	-2
6.5	0	+2	-2	0	+1	+6	-3
7	-1	-2	+1	0	-1	0	0
7.5	+1	-1	-2	-5	0	+1	0
8	0	-1	+1	+2	-2	+3	0
8.5	0	+3	+3	+5	+7	+1	-2
9.1	0	+2	+3	+1	+1	+2	-1
9.5	+1	-4	+1	0	-1	+2	-3
10	+1	0	0	-2	+4	0	0
Maximum	+2	+5	+3	+6	+7	+6	+2
Minimum	-3	-4	-6	-5	-3	-2	-4
Average	0.0	+0.053	-0.44	+0.53	+0.28	+0.37	-1.0

*See Figures A-10 through A-16 For Specific Data

were made using only the fan tuners. Table 4 compares the differences from the reference. It is clear that both tuners can be safely omitted for most cases with no adverse effect on the results. The twisted shielded cable is still the most extreme value.

2.2.2.4 Paddle Wheel Tuners - The logical next step is to try elimination of one of the fan tuners. The enclosure tuner seemed most likely to be removable. It was quickly discovered that the enclosure tuner is very effective in providing necessary tuning, so a more elaborate experiment to define its range of effectiveness was devised. The experiment consisted of rotating the cabinet fan tuner through 360° for a fixed orientation of the enclosure fan. The transferred power was recorded at each 5° rotation increment for the cabinet tuner. The enclosure tuner was then rotated five degrees and the process repeated until the enclosure tuner had been rotated a full revolution (72 steps). The data so obtained can be processed to yield a statistical description of the enclosure tuner effectiveness.

For a fixed position of the enclosure tuner, a probability distribution as shown in figure 4 can be derived. The ordinate is the probability of the measured power exceeding the abscissa value. The peak power (at the lowest probability level) is the power level that is used in the MIL-STD-1377 determination of the shielding effectiveness (this level is compared to the peak value measured from the bare reference wire). The effect of the cabinet tuner as shown by this curve proves that the cabinet tuner is required. When all 72 cases (corresponding to the 72 positions of the enclosure tuner) are plotted together as in figure 5, a qualitative feel for the impact of the enclosure tuner is obtained. The range of values obtained from a set of such measurements (see A-24 through A-33) exceeds 25 dB. It is obvious that the enclosure tuner is required if any reasonable estimate of the optimum tuning condition is to be achieved.

2.2.3 Demonstration of Feasibility of Automation - The purpose of the work described in paragraphs 2.2.1 and 2.2.2 was to decrease the complexity of automating

Table 4 Effect of Elimination of Impedance Tuners

Difference* Between Not Using Impedance Tuners and Using Impedance Tuners

Freq	Calibration Loss	Twisted Shielded Pair	Enclosure #1	Enclosure #2	Enclosure #3	Enclosure #4	Enclosure #5
1 Gliz	0 dB	0 dB	0 dB	0 dB	- dB	-2 dB	-1 dB
1.5	-	-1	-	-	-5	-5	+1
2	+1	-4	-4	-1	-4	-2	-5
2.5	-5	-7	-2	+3	0	-3	-2
3	-2	-7	-2	+8	-1	-1	-3
3.5	-2	-6	+2	-3	-1	-2	0
4	0	-6	-2	0	-3	0	+2
4.5	0	-8	-2	-1	0	+2	+1
5	+1	-4	-6	-2	0	-1	+3
5.6	0	-5	+3	-1	+2	+1	-1
6	+1	-8	0	+2	0	+2	0
6.5	+3	-8	-3	0	+1	+7	+2
7	0	-8	+1	0	-2	0	0
7.5	+1	-7	0	-1	0	0	+2
8	+4	-9	0	-2	-1	+5	-1
8.5	-1	+1	-1	+1	+6	-1	+1
9.1	0	0	+4	+1	+1	+2	-1
9.5	+3	0	0	+3	0	0	-4
10	+1	-1	0	0	+5	+6	0
Maximum	+4	+1	+4	+8	+6	+7	+3
Minimum	-5	-9	-6	-3	-5	-5	-5
Average	+0.22	-4.6	-0.67	+0.39	-0.11	+0.42	-0.32

See Figure A-17 Through A-23 For Specific Data

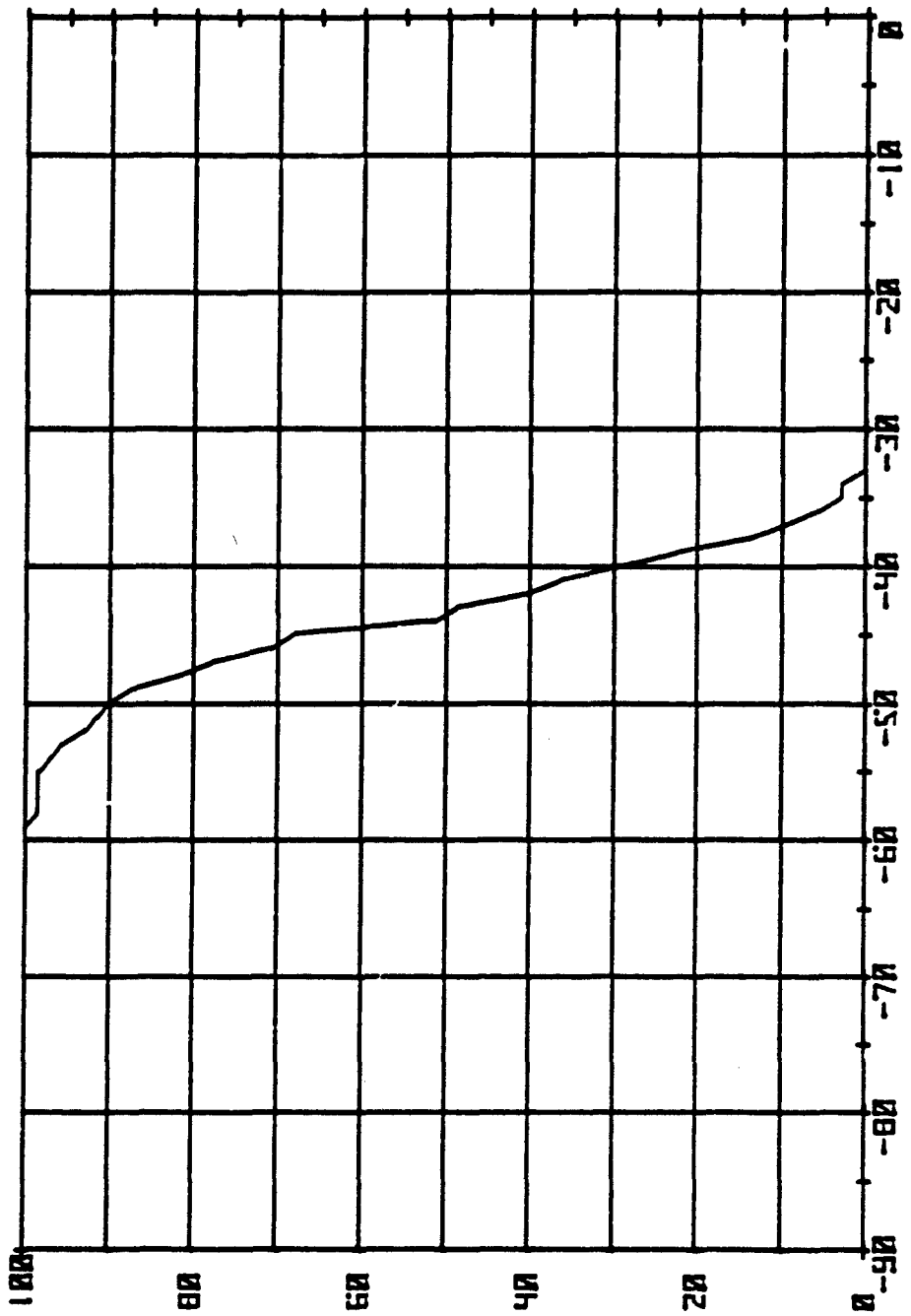

Figure 4 Probability Distribution of Measured Power for Fixed Position of Enclosure Tuner and 360° Rotation of the Cabinet Tuner

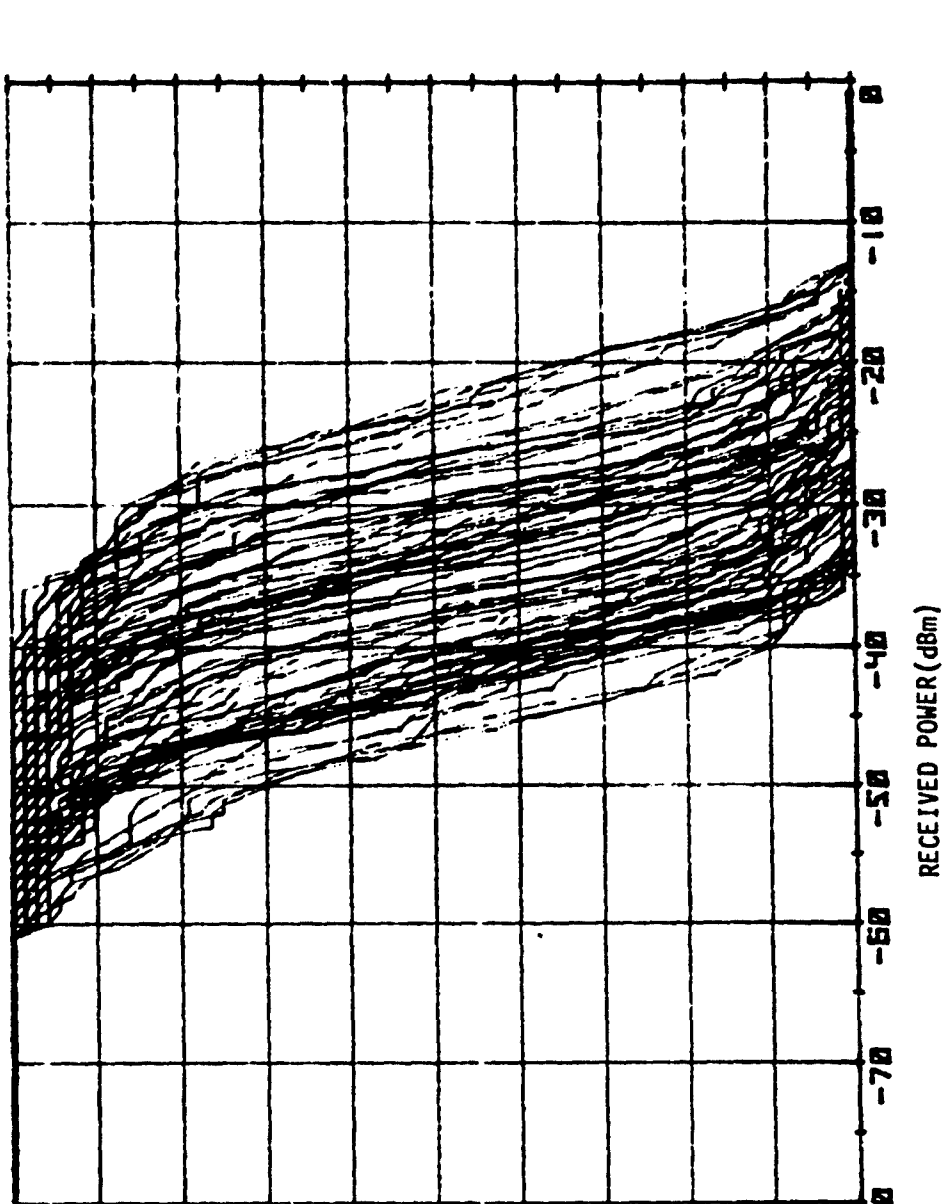

Figure 5 Effect of Internal Paddle Wheel Tuner on Distribution of Shield Loss - Enclosure # 1 at 3 GHz

MIL-STD-1377 shielding effectiveness tests. Invention of the fan tuner requiring rotation only and elimination of the input and output impedance tuners gives enough simplification to demonstrate the feasibility of swept frequency shielding effectiveness measurements using random tuning.

For swept frequency measurements of the enclosures, the signal generator which provided the input power to the modified MIL-STD-1377 chamber, which we call TEMEC (Translational Electromagnetic Environment Chamber), was swept from 2.1 Ghz to 4 GHz at a rate of 100 sweeps per second. The cabinet fan tuner was rotated at approximately one revolution per second and the enclosure fan tuner rotated at approximately two revolutions per second. A spectrum analyzer with a variable persistence screen was used as a receiver and swept from 2.1 GHz to 4.0 GHz at 2 seconds per division (20 seconds per trace). Figure 6 shows pnotographs of the spectrum analyzer traces necessary to provide the data. The top photograph is the reference, i.e.; the received signal for a hard wire connection from signal generator to spectrum analyzer, bypassing the TEMEC chamber. The middle photograph is the cabinet calibration signal; i.e., the received signal at the bare reference wire when applying the generator signal to the transmitting antenna in the TEMEC chamber while rotating the cabinet tuner. The bottom photograph is the shield loss signal; the received signal at the test specimen when applying the generator signal to the transmitting antenna while rotating both fan tuners. Three sweeps of the spectrum analyzer were stored before taking a photograph, so the random tuning was performed for one minute for each photograph. A longer time period would provide a greater probability of recording the maximum signal in each frequency interval, but we were limited by the characteristics of the spectrum analyzer variable persistence screen (the screen "blooms" for long exposures). When large frequency ranges are displayed as they were here, discrete frequency data is subject to

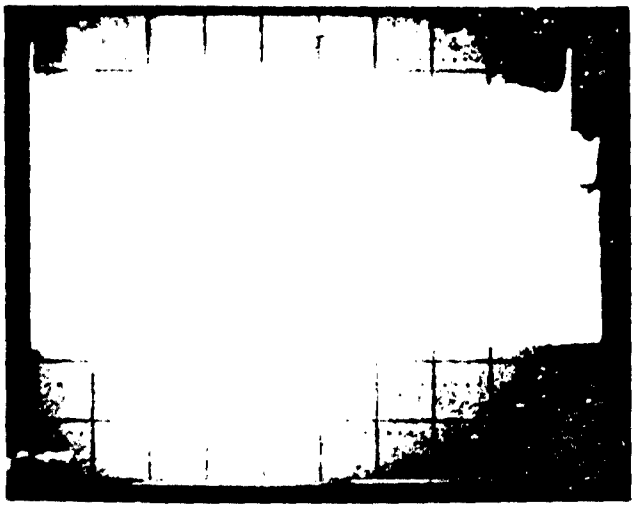

a) Reference Signal

b) Calibration Signal

c) Shield Loss Signal

Figure 6
Swept Frequency Measurement of
Enclosure # 5 Shielding Effectiveness
Vertical = 10 dB/div.
Horizontal = 200 MHz/div.

uncertainties in reading the values, but we have compared in table 5 the swept frequency results to the manual tuning results obtained earlier for five enclosures and one shielded cable. Considering the uncertainties in reading specific data points from the photographs, the results are considered to demonstrate the feasibility of the random tuning concept.

Since processing the data requires subtracting values in the shield loss photograph from those in the cabinet calibration photograph, this technique is not promising due to the problem of manually reading the data. A more practical technique appears to be use of a computer controlled system to measure shielding effectiveness for finely spaced frequency increments.

2.3 Extension of TEMEC Techniques to Absolute Coupling Measurements - Shielding effectiveness measurements are relative and cannot supply complete coupling measurements in themselves. Presently, the means for providing an absolute link between the radiated EM environment and the pickup power is through measurement of effective aperture in a free field, usually in an anechoic chamber. If it is possible to calibrate the TEMEC chamber for absolute coupling measurements, then even the anechoic chamber measurements of effective aperture can be replaced by the more economical TEMEC measurements.

Following measurements to find the useful volume of the TEMEC chamber, we conducted experiments to determine a calibration factor establishing the relationship between TEMEC absolute coupling and anechoic chamber measurements. Coupling factors were calculated; however, additional anechoic chamber measurements to determine the distribution of coupling data due to internal tuning are required to determine if the technique is accurate enough to be usable.

Table 5 Swept Frequency Measurements* Sampled at Discrete Points and Compared to Manual Measurements

	Frequency (GHz)			
	2	2.5	3	3.5
Enclosure 1				
Swept Frequency S.E.	4	7	15	20
Manual S.E.	7	8	12	12
Difference	-3	-1	3	8
Enclosure 2				
Swept Frequency S.E.	17	6	15	26
Manual S.E.	22	7	11	15
Difference	-5	-1	4	11
Enclosure 3				
Swept Frequency S.E.	17	9	5	8
Manual S.E.	6	6	13	11
Difference	11	3	-8	-3
Enclosure 4				
Swept Frequency S.E.	17	9	5	8
Manual S.E.	6	6	13	11
Difference	11	-3	-8	-3
Enclosure 4				
Swept Frequency S.E.	22	18	14	18
Manual S.E.	13	8	13	12
Difference	9	10	1	6
Enclosure 5				
Swept Frequency S.E.	26	23	18	15
Manual S.E.	26	11	6	8
Difference	0	12	12	7

360° Twisted Shielded Pair	4.5 GHz	5 GHz	5.5 GHz	6 GHz
Swept Frequency S.E.	40	45	40	33
Manual S.E.	42	38	36	37
Difference	-2	7	4	-4

* See Figure A-34 Through A-38 For Photographs

2.3.1 Useful Volume of TEMEC Chamber - To determine the useful volume of the TEMEC chamber, the maximum power density was mapped over the volume of the chamber. A Narda Model 8305 Broadband Isotropic Radiation Monitor with a Narda Model 8321 Isotropic Probe was used to do this. The maximum power density was measured with the probe at many different locations in the chamber. The chamber is 3 feet wide by 5 feet long by 3 feet high. The maximum power density for each location was found by rotating the fan and noting the peak reading. The data are shown in Figures 7 and 8. In these figures the units are power per unit area for a constant power input and have been normalized to the average value measured.

The data indicates that the maximum power density varies 6.6 dB (10 log 2.24/.49) at 3 GHz and 2.82 dB (10 log 1.44/.77) at 9.1 GHz over the volume of the chamber.

2.3.2 TEMEC Chamber Calibration for Power Density - An attempt to calibrate the TEMEC chamber was made in two ways. The first utilized the Narda probe as a standard for measuring power density in the TEMEC chamber and the calibration factor would be a table showing power input required to obtain a particular power density in the TEMEC chamber. The second involves relating input power to the TEMEC chamber to power density in the anechoic chamber by comparing values of power coupled onto an unshielded wire for each test. The validity of the two techniques was tested using the results of TEMEC and anechoic chamber measurements for a bare wire and for five enclosures. Available data indicates that the first technique is not valid, but the second technique appears viable.

2.3.2.1 Calibration Using Narda Probe - The Narda Probe was placed in the TEMEC chamber and the fan rotated to give maximum power density. Table 6 shows the maximum power density for a fixed input power over 1.5 - 10 GHz.

To test the validity of this calibration, an unshielded wire was placed in the TEMEC chamber, and the distribution of received power measured by rotating the fan and recording pick up power every 5° through 360° of rotation at 3 GHz,

5'

3'

1.34	1.34	0.90	0.67	1.72	0.57	2.24	1.57	1.12	1.34
1.34	1.34	1.25	1.16	0.72	1.12	0.90	1.12	0.81	0.90
0.99	0.90	1.34	1.34	0.90	0.90	1.25	0.90	0.90	
1.12	1.34	0.90	0.90	0.76	0.81	0.90	0.90	0.90	FAN
1.25	0.90	0.90	1.34	0.90	1.79	0.90	1.12	0.90	
1.34	0.90	0.90	0.85	1.43	0.90	0.90	1.25	0.99	
0.99	1.79	0.99	0.72	1.43	1.25	1.25	0.90	0.90	0.99
0.90	0.76	0.81	0.99	1.34	1.12	1.12	0.90	1.34	1.43

a) Field Distribution at Height of 15 Inches From Bottom of Chamber

0.99	1.12	0.90	0.99	0.90	1.25	0.90	1.12	0.90	1.12
1.34	1.12	0.90	0.67	0.67	0.90	1.12	1.25	0.90	0.90
0.90	0.81	0.90	0.90	0.90	0.49	0.90	0.99	1.34	
0.76	0.90	0.90	0.90	1.25	1.57	1.57	0.90	0.85	FAN
0.90	0.90	1.12	1.34	1.79	1.12	1.12	1.12	0.99	
0.90	0.90	0.90	1.12	0.90	0.49	0.49	0.90	0.90	
1.03	0.72	0.67	0.99	1.34	0.85	1.25	0.90	0.90	0.90
1.34	0.81	1.25	0.99	1.34	0.67	0.99	0.90	1.79	0.90

b) Field Distribution at Height of 21.5 Inches From Bottom of Chamber

0.90	0.90	0.90	0.90	0.99	0.81	0.90	0.90	0.90	0.90
0.90	0.67	1.34	0.90	0.99	0.90	0.90	0.90	0.67	0.81
0.99	0.90	0.90	0.81	1.34	0.99	0.90	0.67	1.12	
0.90	0.90	1.12	0.67	0.90	0.99	0.90	0.67	0.90	FAN
0.90	0.90	0.99	0.99	1.12	0.90	0.99	1.25	0.90	
0.90	0.90	0.90	0.90	0.63	0.63	0.90	0.90	0.90	
0.90	0.99	1.12	0.81	0.90	0.90	1.34	0.99	0.90	0.81
0.90	1.25	0.81	0.99	1.12	0.99	0.85	0.85	0.81	0.90

c) Field Distribution at Height of 26 Inches From Bottom of Chamber

Figure 7 TEMEC Chamber Mapping at 3 GHz

5'

3'

0.86	1.34	1.15	0.82	0.96	1.01	0.96	0.91	1.44	1.15
1.06	0.96	1.25	0.91	0.91	0.82	1.01	1.25	0.77	0.96
1.15	0.91	0.86	1.06	0.96	1.01	0.96	0.96	0.91	
1.25	0.77	1.06	0.82	0.82	0.96	0.82	0.96	0.86	FAN
0.86	0.96	0.96	0.86	0.77	0.82	0.82	0.82	1.34	
1.06	1.06	0.91	0.86	1.30	0.82	0.96	0.82	0.91	
1.34	1.01	0.82	0.96	0.91	0.77	0.86	1.01	1.06	1.06
1.34	1.06	1.06	1.34	0.96	1.06	0.96	1.30	1.20	1.06

a) Field Distribution at Height of 21.5 Inches From Bottom of Chamber

1.06	1.01	1.25	1.20	0.82	0.91	0.96	0.91	1.44	0.91
1.06	1.15	1.06	1.20	0.86	0.91	1.15	1.06	0.86	1.01
1.01	0.91	0.86	1.06	0.86	0.86	0.91	0.91	1.06	
1.10	1.06	0.96	1.44	1.01	0.96	0.82	0.82	0.86	FAN
0.96	0.82	1.06	1.44	1.44	1.15	0.82	0.82	0.86	
1.06	1.15	0.82	0.77	1.06	0.91	0.86	0.82	0.96	
0.86	0.96	0.77	1.01	0.91	0.96	0.82	0.82	1.25	1.06
0.91	0.82	1.15	0.96	0.96	0.96	1.54	1.15	1.34	0.86

b) Field Distribution at Height of 26 Inches From Bottom of Chamber

Figure 8 TEMEC Chamber Mapping at 9.1 GHz

Table 6 TEMEC Chamber Calibration Using Narda Probe

FREQUENCY (GHZ)	INPUT POWER (mW)	POWER DENSITY $(\frac{mW}{cm^2})$
1.5	100 mW	2.4
2	100 mW	4.5
2.5	100 mW	2.0
3	100 mW	2.2
3.5	100 mW	1.5
4	100 mW	1.6
4.5	100 mW	5.0
5	100 mW	2.5
5.5	100 mW	5.6
6	100 mW	5.0
6.5	100 mW	8.5
7	100 mW	4.0
7.5	100 mW	4.5
8	100 mW	5.5
8.5	100 mW	5.8
9	100 mW	9
9.5	100 mW	6
10	100 mW	3

5.6 GHz, and 9.1 GHz. The results are shown in figures 9 through 11 after normalizing for a power density of 1 W/M^2 using table 6. Also shown are the results of anechoic chamber measurements on an unshielded wire. The separation is only 3 dB at 3 GHz, but it is 12 dB at 9.1 GHz. Thus, the power densities in the TEMEC as measured by the Narda probe do not permit prediction of the coupled power very accurately.

2.3.2.2 Calibration Using Unshielded Wire Data - To calibrate the TEMEC chamber using pickup by an unshielded wire in an anechoic chamber as a standard, the distribution of received power in both the TEMEC chamber and anechoic chamber data are used. Table 7 shows how this is done at the three frequencies for which we have both TEMEC and anechoic chamber data on an unshielded wire. For example, at 3 GHz the average pickup for the unshielded wire was -0.2 dBm for +20 dBm input power to the TEMEC chamber. The average pickup in the anechoic chamber was -13.8 dBm for a 1 W/M^2 field. In order to create an equivalent 1 W/M^2 field in the TEMEC chamber, the input power must be reduced by 13.6 dB [-0.2 - (-13.8)] so that the unshielded wire will receive the same power in either the TEMEC or anechoic chamber.

In effect, the two curves in each of figures 9 through 11 are made to coincide at their average and it can be seen that the parallelism supports the analogy that TEMEC conditions simulate the anechoic chamber conditions. To determine the generality of this calibration factor, the data from the distribution of received power discussed in paragraph 2.2.2.4 for the five enclosures may be used in conjunction with the calibration factors just derived. The TEMEC data for enclosure #1 showing the variation to be expected in enclosure measurements due to internal conditions is shown in figure 12. In this figure TEMEC MAX is a trace of the envelope representing maximum pickup and TEMEC MIN represents the minimum pickup boundary. Also shown is a plot of the anechoic chamber measurements for the one internal condition for which data is available for this configuration.

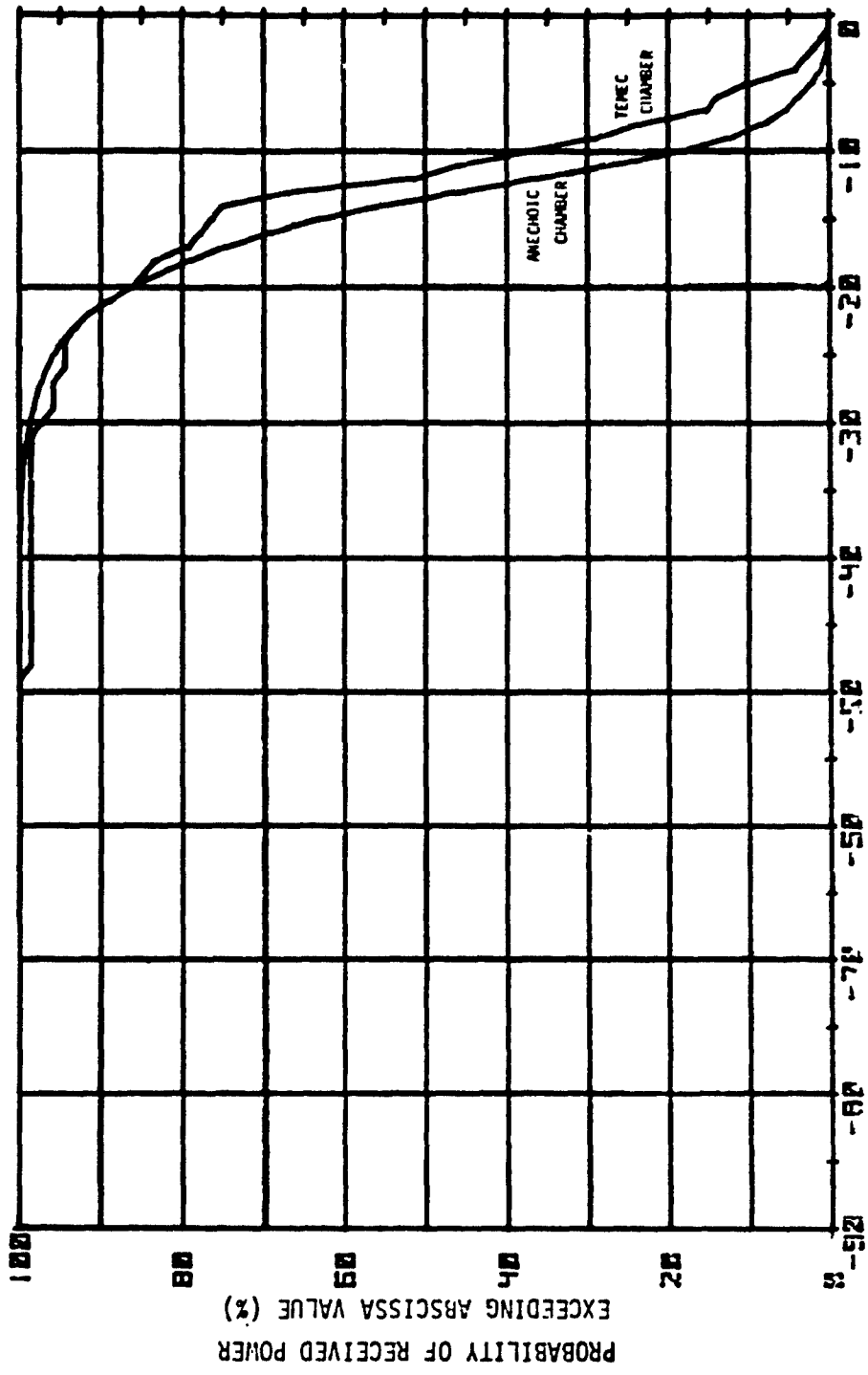

Figure 9 Comparison of Anechoic Chamber and TEMEC Chamber - Distribution of Pickup by Bare Wire Exposed to 1 W/M^2 Power Density at 3.0 GHz

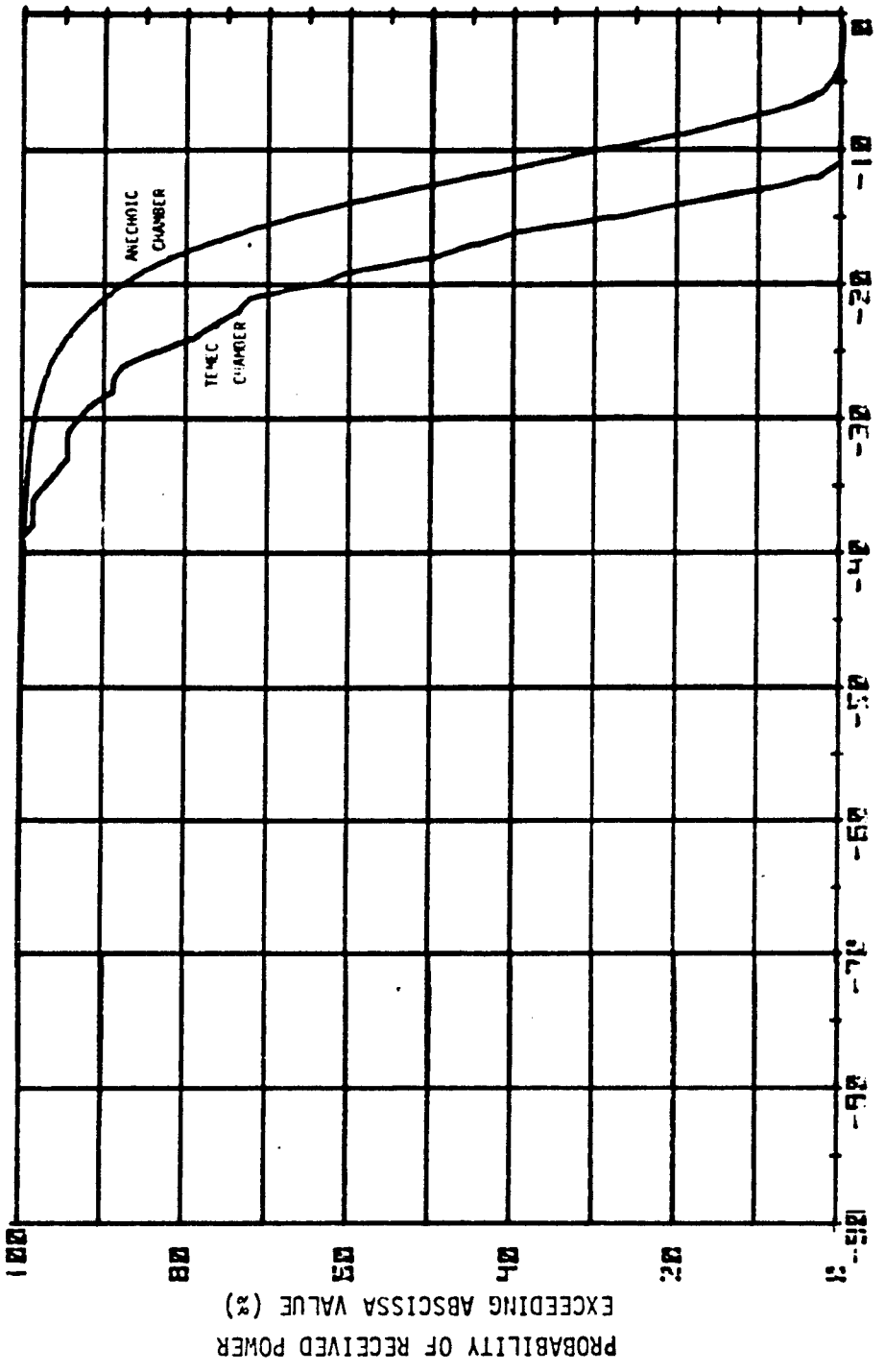

Figure 10 Comparison of Anechoic Chamber and TEMEC Chamber - Distribution of Pickup by Bare Wire Exposed to 1 W/M^2 Power Density at 5.6 GHz

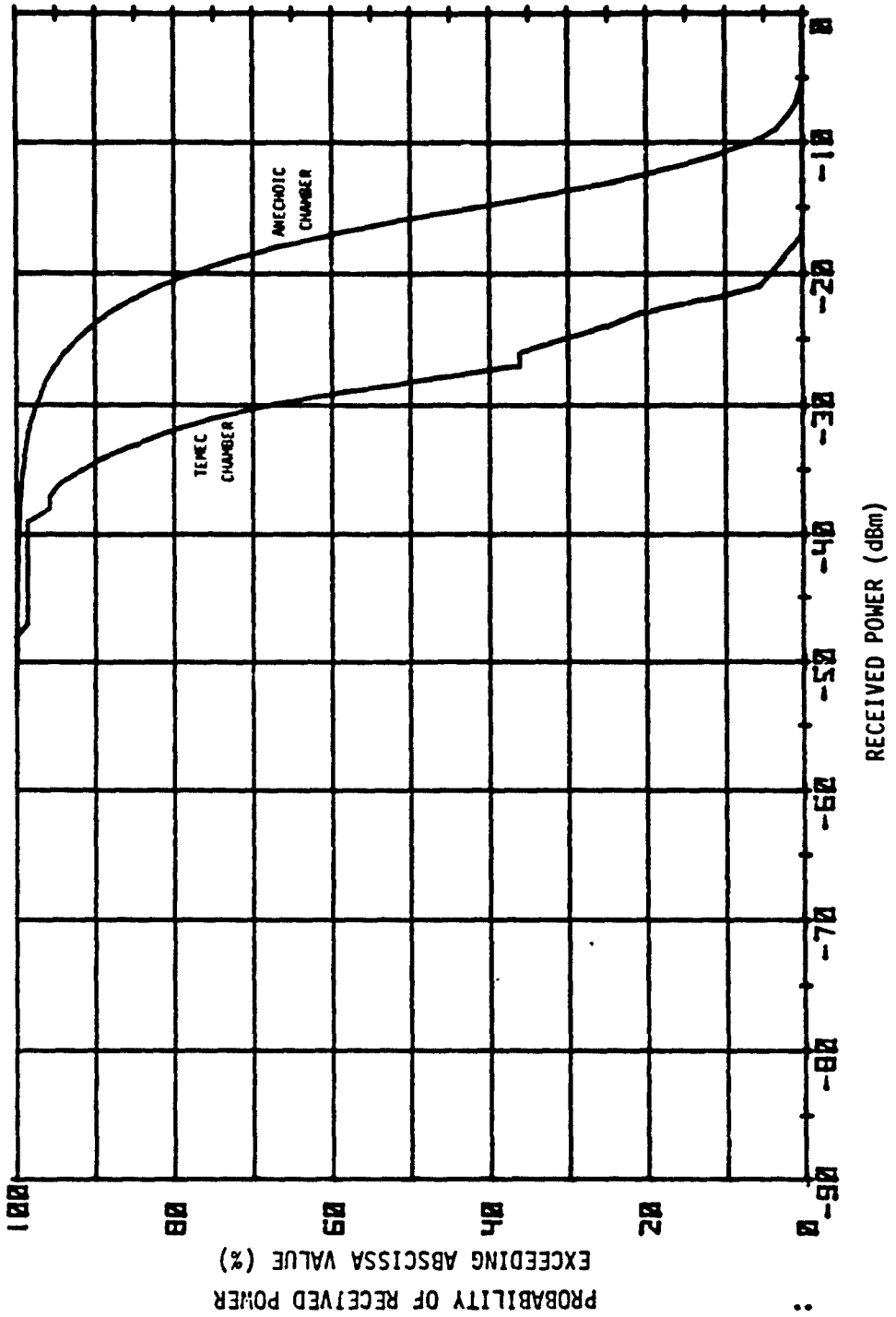

Figure 11 Comparison of Anechoic Chamber and TEMEC Chamber - Distribution of Pickup by Bare Wire Exposed to 1 W/M^2 Power Density at 9.1 GHz

Table 7 Calibration of TEMEC Chamber Using Unshielded Wire Data

Frequency (GHz)	P_{IN}(TEMEC)	$\overline{P}_R$(TEMEC)	$\overline{P}_R$ (Anechoic Chamber for 1 W/M^2 Field)	Correction Factor	($TEMEC_2$ for P_{IN} 1 W/M^2 Field)
3	+20 dBm	-.2 dBm	-13.8 dBm	13.6 dB	6.4 dBm
5.6	+20 dBm	-2.8 dBm	-13.2 dBm	11.4 dB	10.6 dBm
9.1	+20 dBm	-8.5 dBm	-15.9 dBm	7.4 dB	12.6 dBm

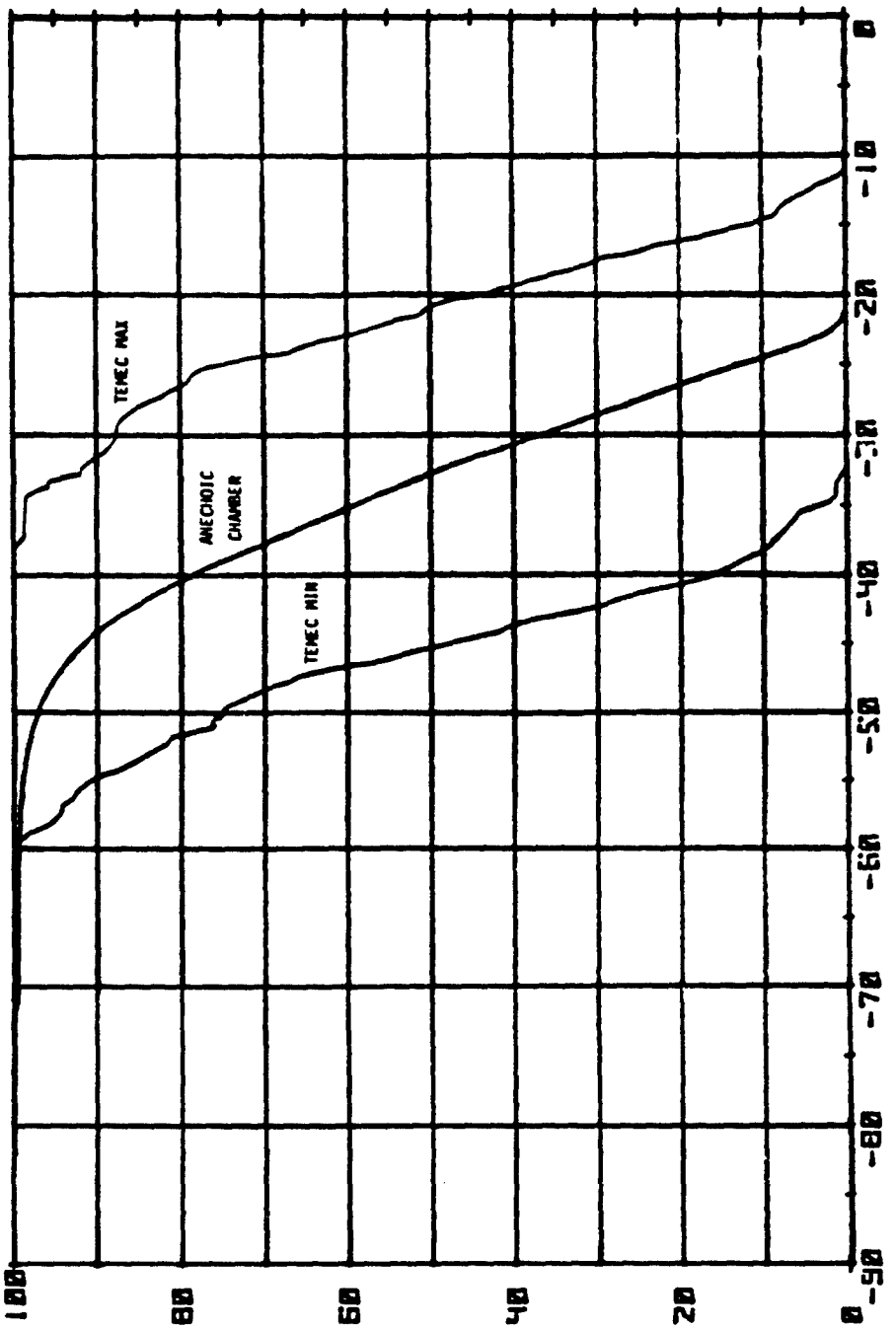

Figure 12 Comparison of TEMEC to Anechoic Chamber Measurement of Distribution of Received Power - Enclosure # 1 at 3 GHz in 1 W/M^2 Field

Similar curves for ten additional configurations are shown in Figures A-39 through A-48. In almost all the figures the curve representing the anechoic chamber data for one internal tuning condition falls comfortably within the boundary curves from the TEMEC measurements; thus, indicating that the calibration technique is valid. However, no final conclusions can be reached as to the use of this calibration technique or even for the use of the TEMEC chamber for absolute coupling measurements until additional anechoic chamber data is made available and examined. We also emphasize that calibration factors derived in this manner will probably have to be obtained for each individual TEMEC chamber, especially for different sized chambers.

3. Conclusions and Recommendations

The feasibility of automating the MIL-STD-1377 shielding effectiveness technique was successfully demonstrated following simplification of the MIL-STD-1377 tuning technique. Paddle wheel tuners were fabricated which permit tuning using rotational motion only, and several experiments were performed which indicated that both the input and output impedance tuners can be omitted for enclosure measurements and the input tuner can be omitted for cable measurements. These experiments also indicated that both the enclosure and cabinet paddle wheel tuners are required for enclosure shielding effectiveness measurements. The field intensity in the MIL-STD-1377 chamber was mapped and the useful volume determined to be approximately equal to the physical volume. Experiments performed to investigate the feasibility of performing absolute coupling measurements in TEMEC (the modified MIL-STD-1377 chamber) were inconclusive due to lack of sufficient anechoic chamber data for comparison. The ahechoic chamber data available, however, does fall within the range of data resulting from measurements in the TEMEC chamber.

Improved data collection techniques for swept frequency measurements, possibly using peak detection and computer storage, should be investigated. Additional anechoic chamber measurements on enclosures should be performed for a variety of enclosure internal tuning conditions and the results compared to the TEMEC measurements to verify TEMEC use for absolute coupling measurements. The possible savings of both time and money in performing absolute coupling measurements in the TEMEC chamber justifies further investigation.

APPENDIX

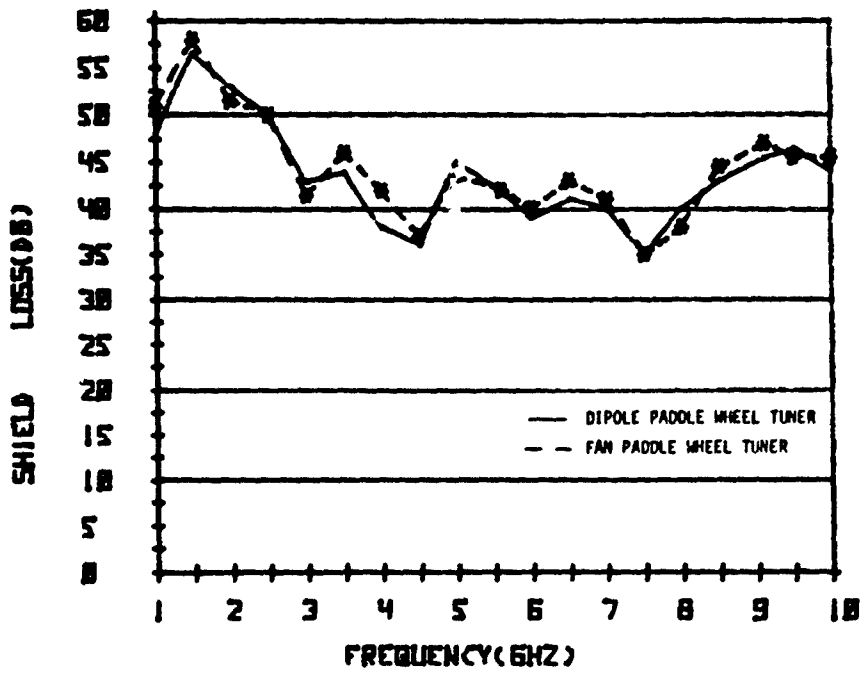

Figure A-1 Comparison of Dipole Paddle Wheel Tuner to Fan Paddle Wheel Tuner Measuring Shield Loss of 360 Degree Shielded Twisted Pair

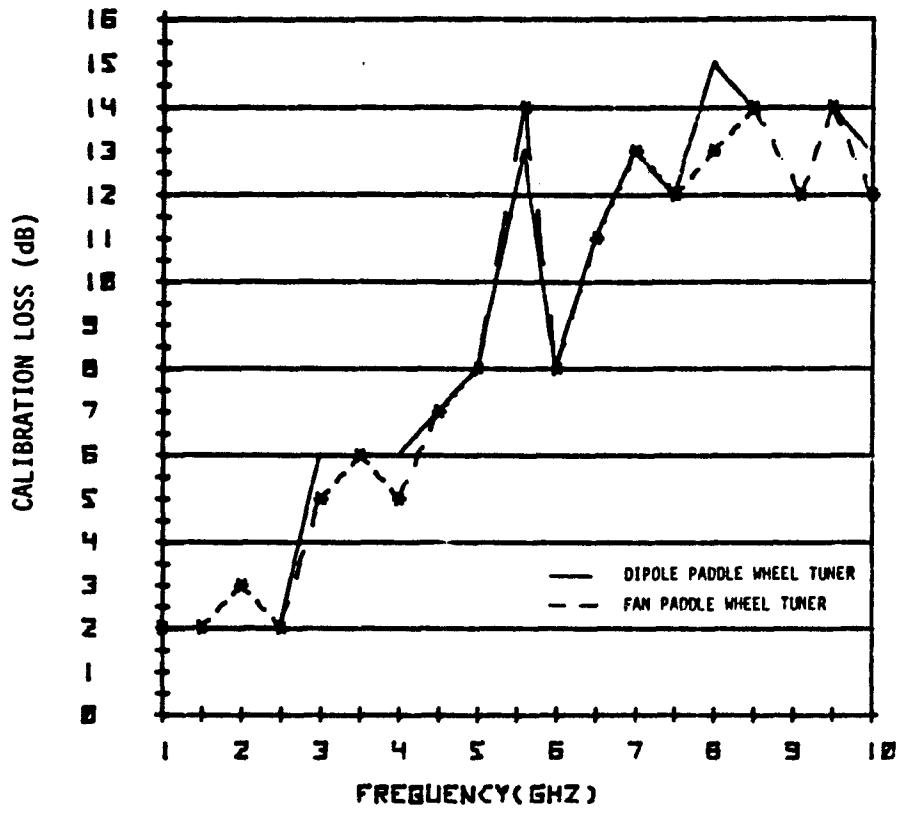

Figure A-2 Comparison of Dipole Paddle Wheel Tuner to Fan Paddle Wheel Tuner Measuring Loss of MIL-STD-1377 Chamber

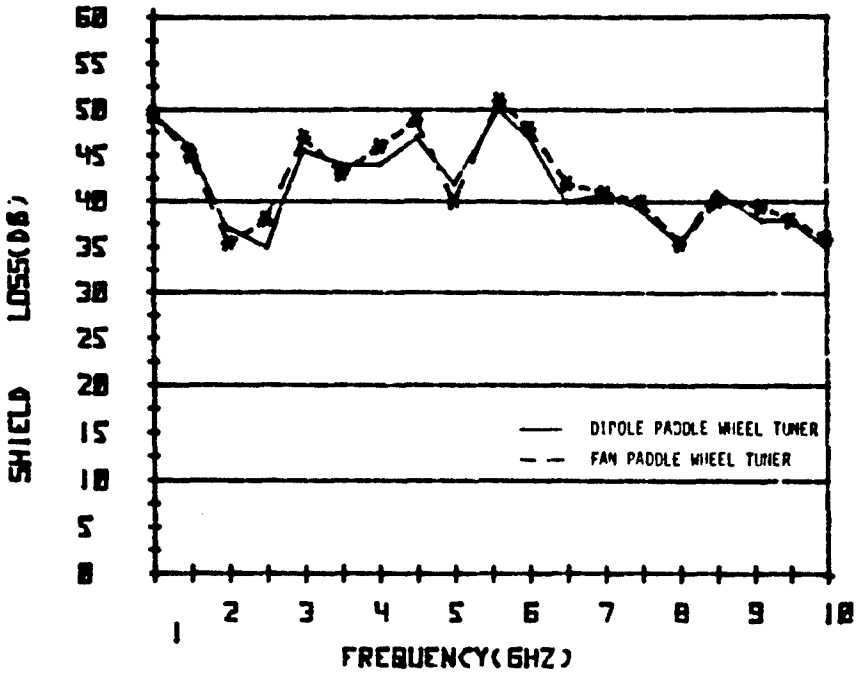

Figure A-3 Comparison of Dipole Paddle Wheel Tuner to Fan Paddle Wheel Tuner Measuring Shield Loss of RG-8/U Cable

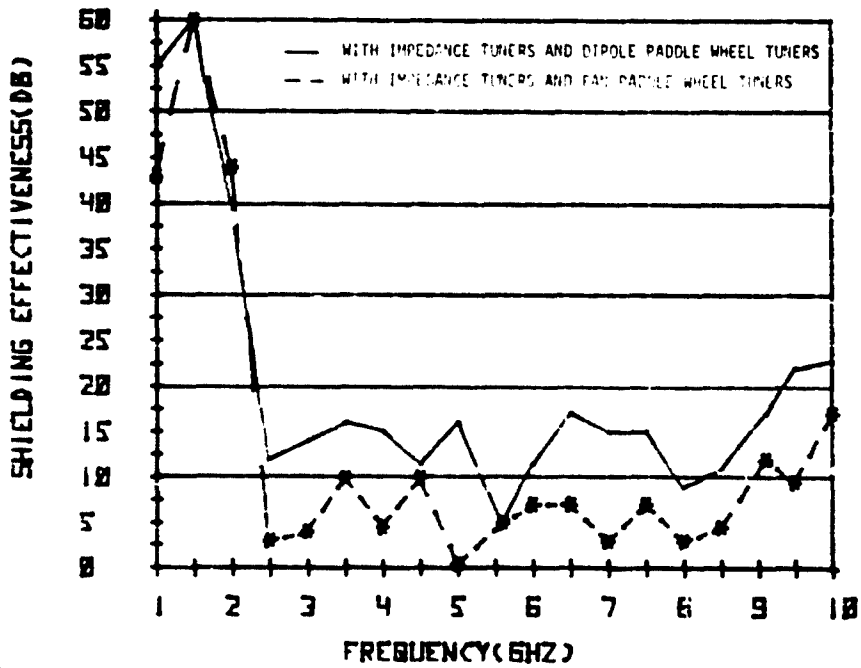

Figure A-4 Comparison of Fan Tuner to Dipole Tuner Measuring Shielding Effectiveness of Enclosure # 1

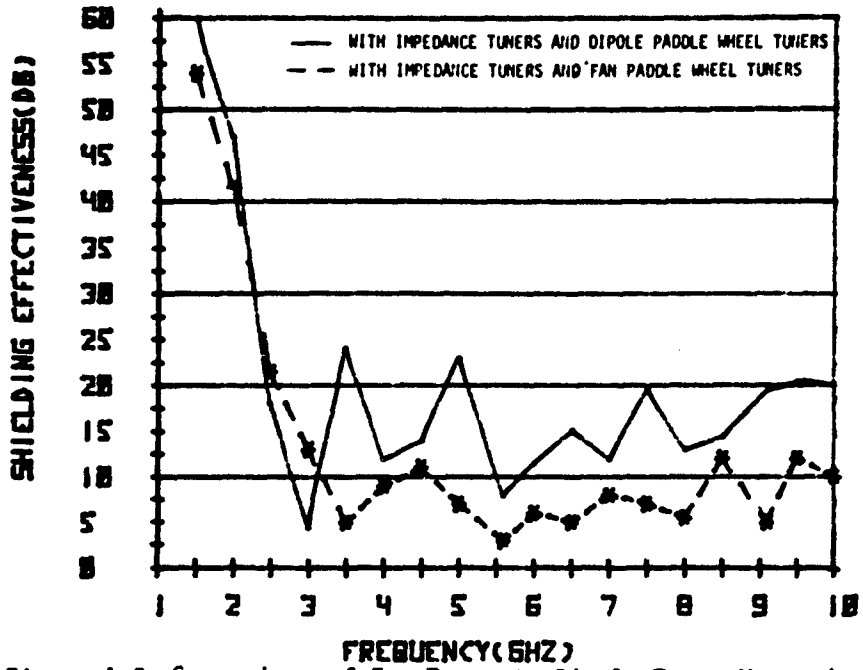

Figure A-5 Comparison of Fan Tuner to Dipole Tuner Measuring Shielding Effectiveness of Enclosure # 2

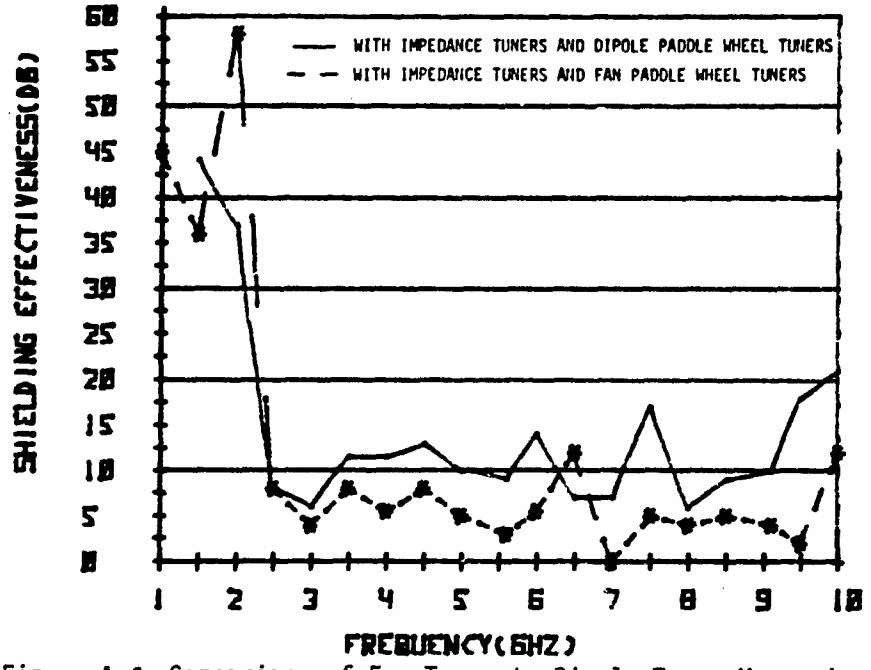

Figure A-6 Comparison of Fan Tuner to Dipole Tuner Measuring Shielding Effectiveness of Enclosure # 3

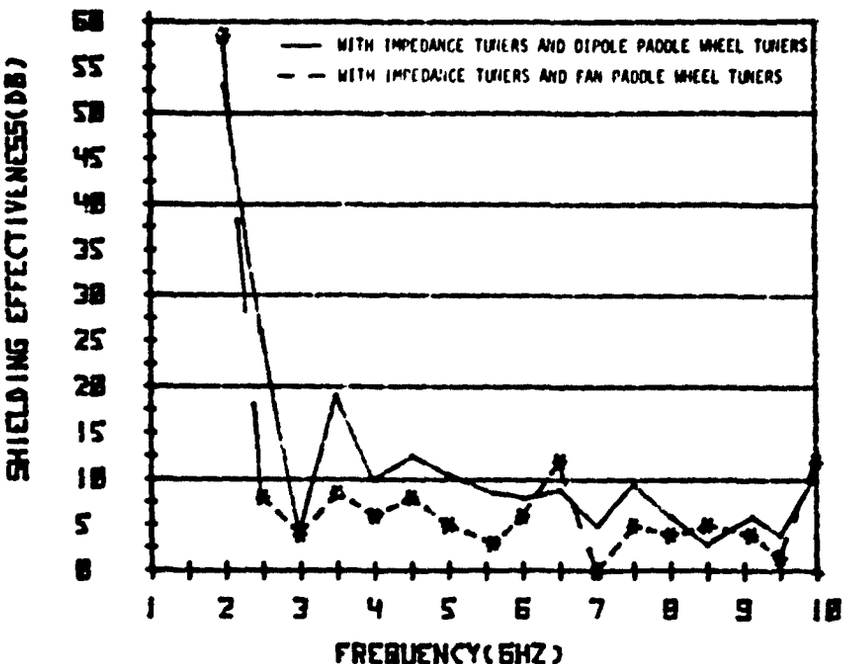

Figure A-7 Comparison of Fan Tuner to Dipole Tuner Measuring Shielding Effectiveness of Enclosure # 4

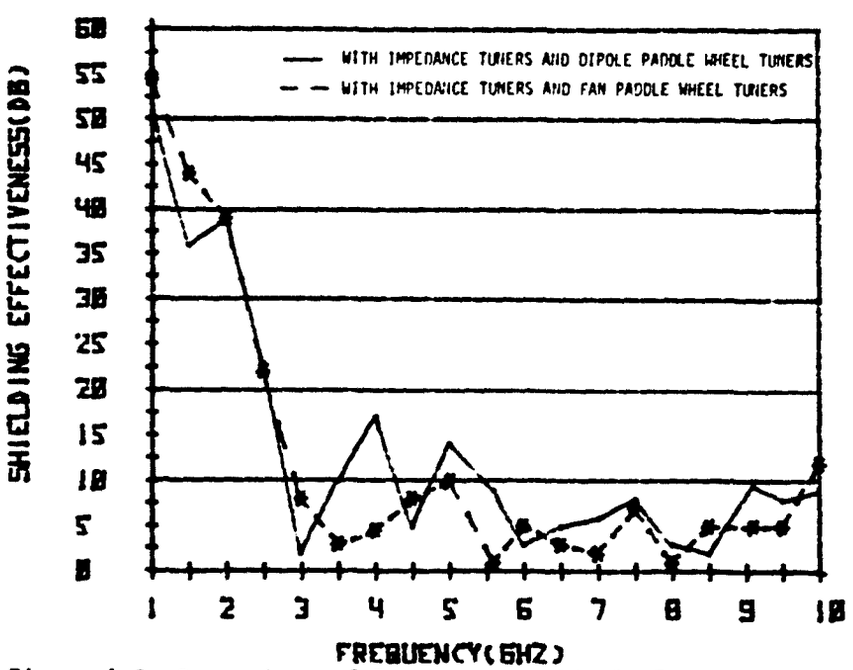

Figure A-8 Comparison of Fan Tuner to Dipole Tuner Measuring Shielding Effectiveness of Enclosure # 5

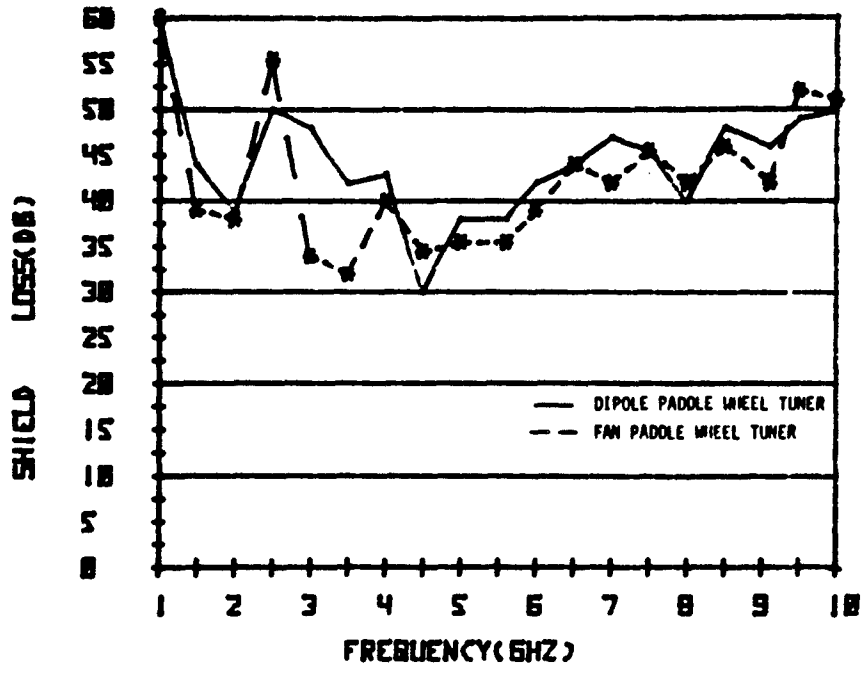

Figure A-9 Comparison of Dipole Paddle Wheel Tuner to Fan Paddle Wheel Tuner Measuring Shield Loss of Aluminum Wire Knit Gasket

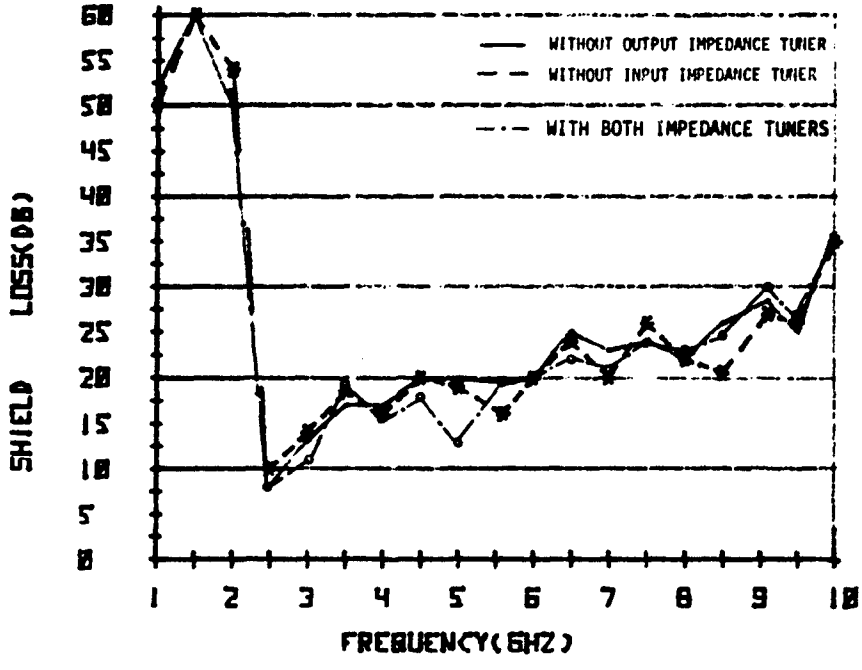

Figure A-10 Effect of Impedance Tuners on Shield Loss of Enclosure # 1

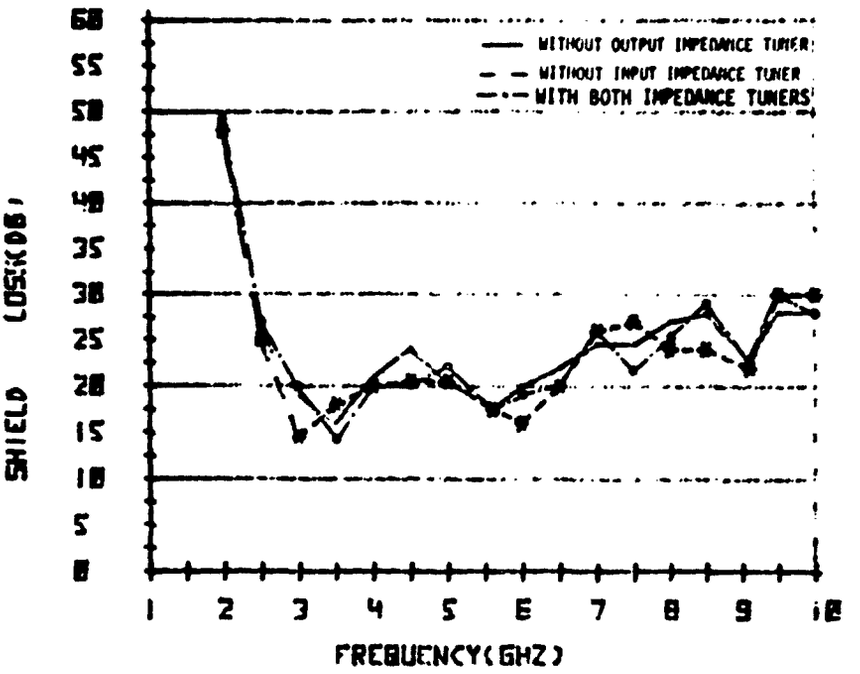

Figure A-11 Effect of Impedance Tuners on Shield Loss of Enclosure # 2

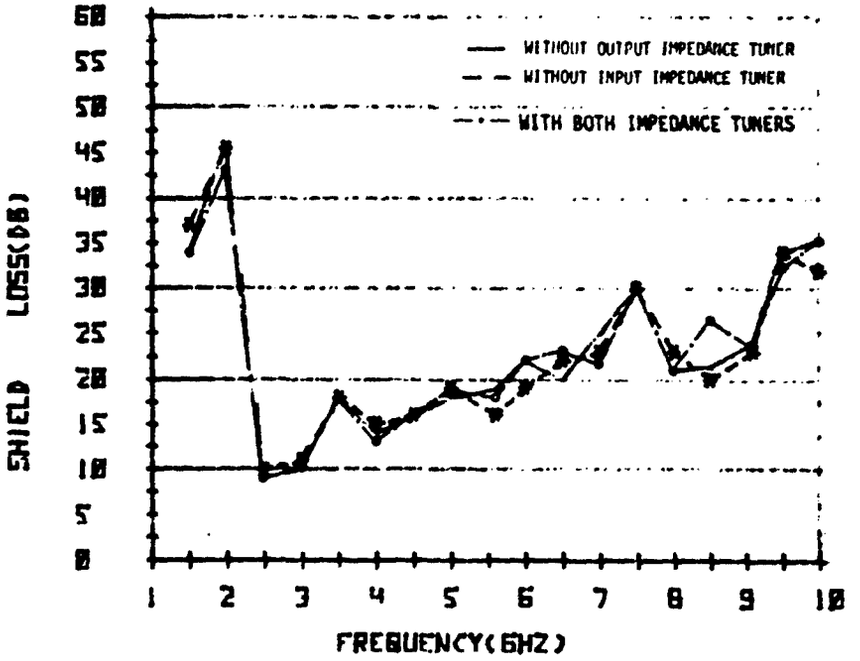

Figure A-12 Effect of Impedance Tuners on Shield Loss of Enclosure # 3

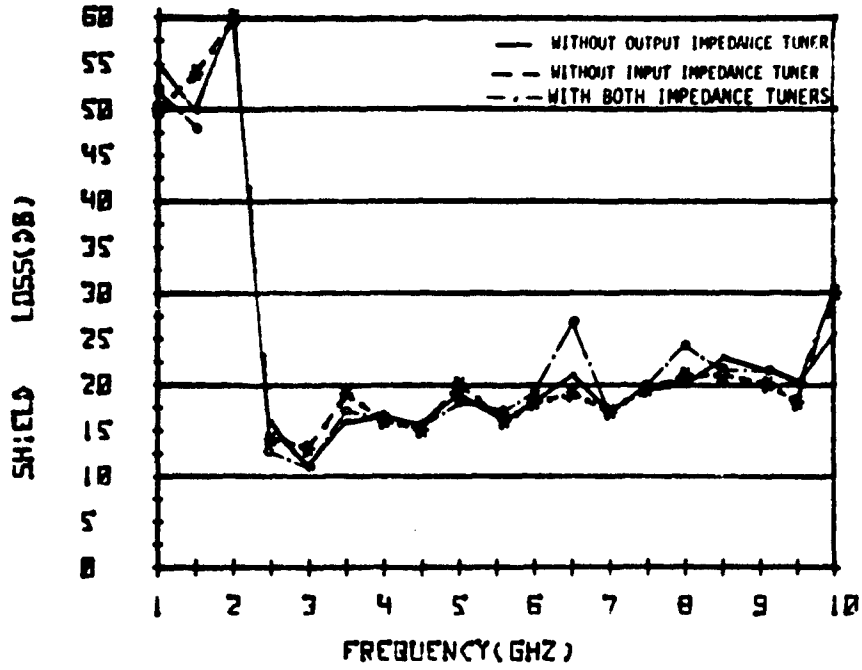

Figure A-13 Effect of Impedance Tuners on Shield Loss of Enclosure # 4

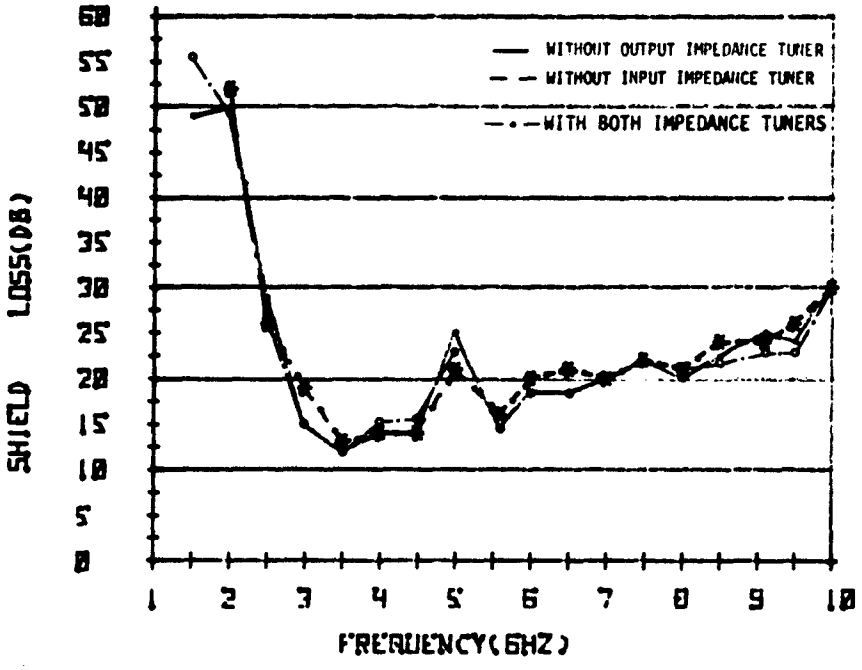

Figure A-14 Effect of Impedance Tuners on Shield Loss of Enclosure # 5

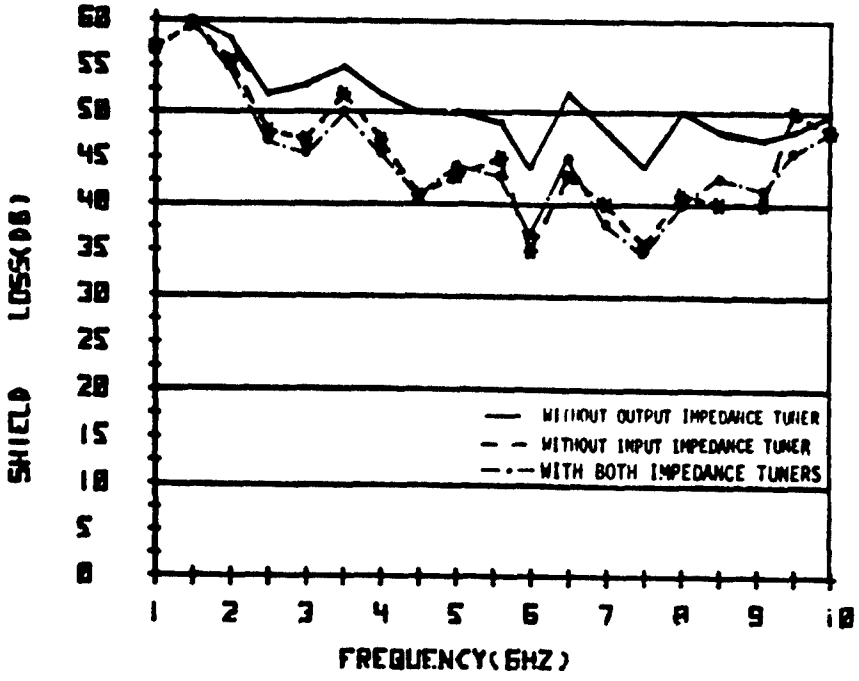

Figure A-15 Effect of Impedance Tuners on Shield Loss of 360 Degree Shielded Twisted Pair

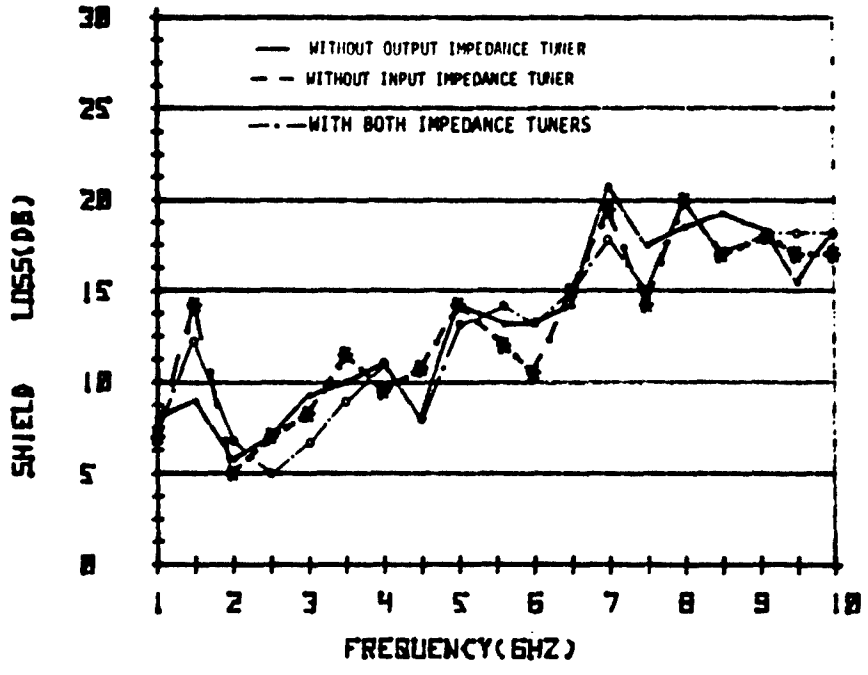

Figure A-16 Effect of Impedance Tuners on Calibration Loss of MIL-STD-1377 Chamber

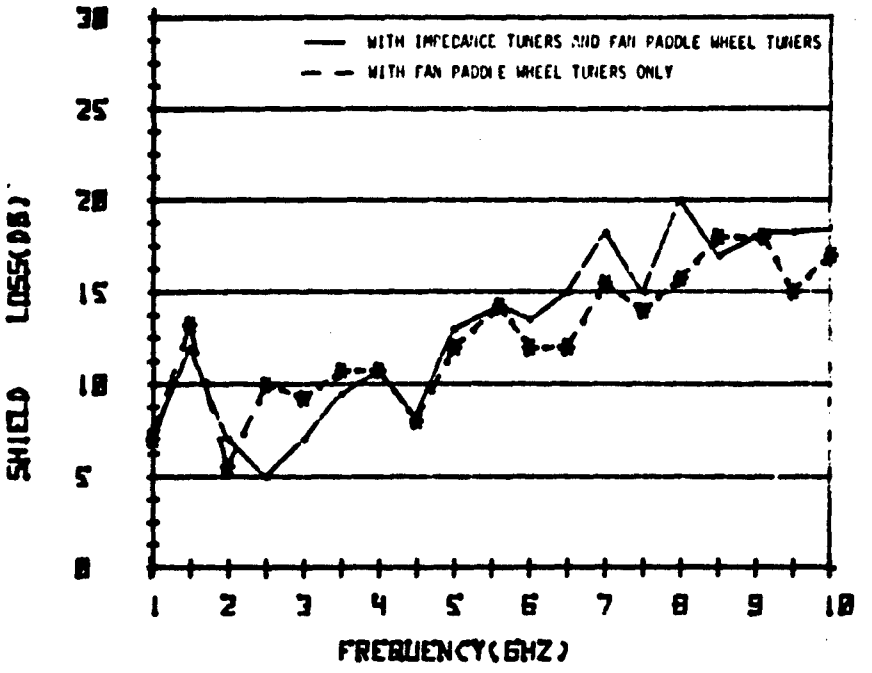

Figure A-17 Effect of Eliminating Impedance Tuners on Calibration Loss of MIL-STD-1377 Chamber (Enclosure # 4 and Narda Probe in Chamber)

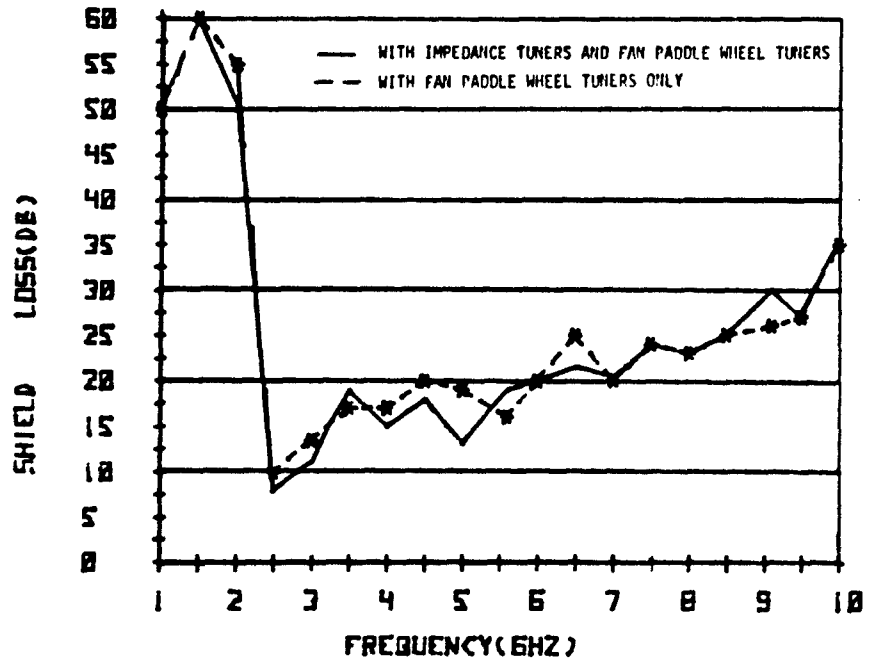

Figure A-18 Effect of Eliminating Impedance Tuners on Shield Loss of Enclosure # 1

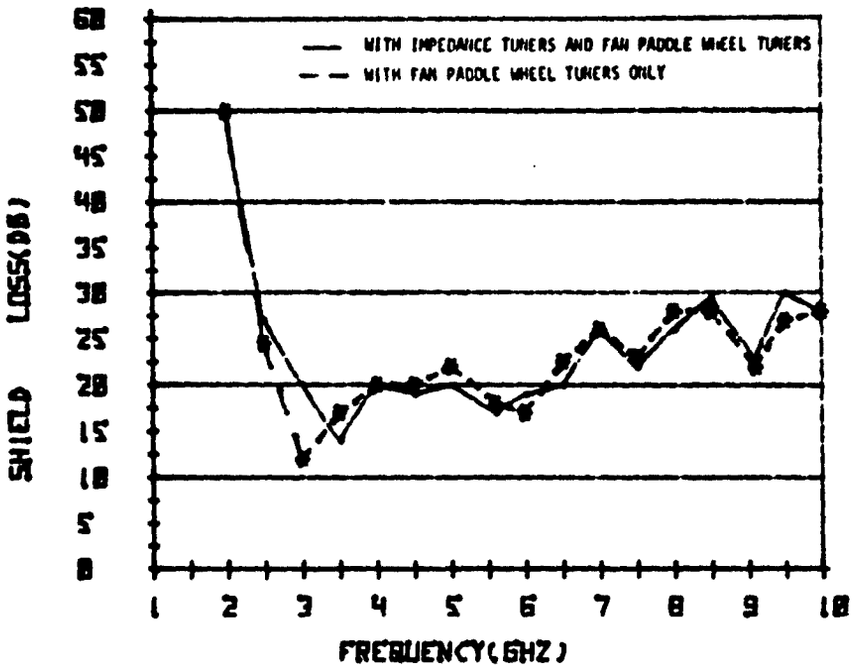

Figure A-19 Effect of Eliminating Impedance Tuners on Shield Loss of Enclosure # 2

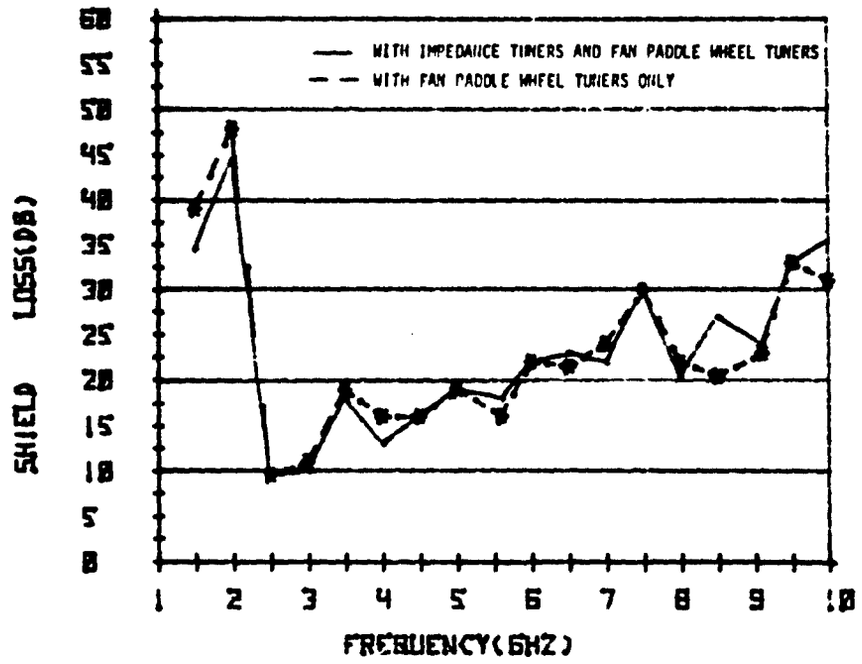

Figure A-20 Effect of Eliminating Impedance Tuners on Shield Loss of Enclosure # 3

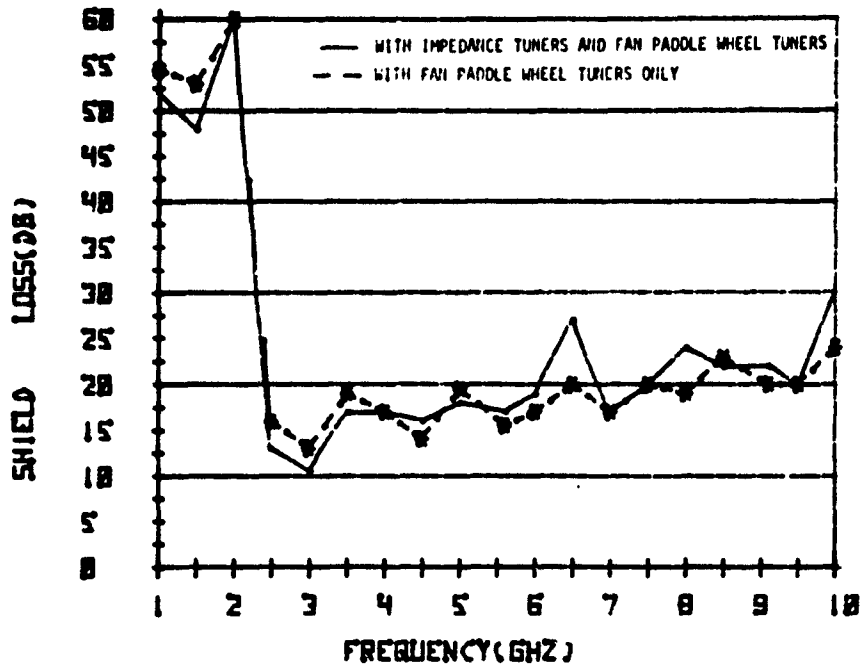

Figure A-21 Effect of Eliminating Impedance Tuners on Shield Loss of Enclosure # 4

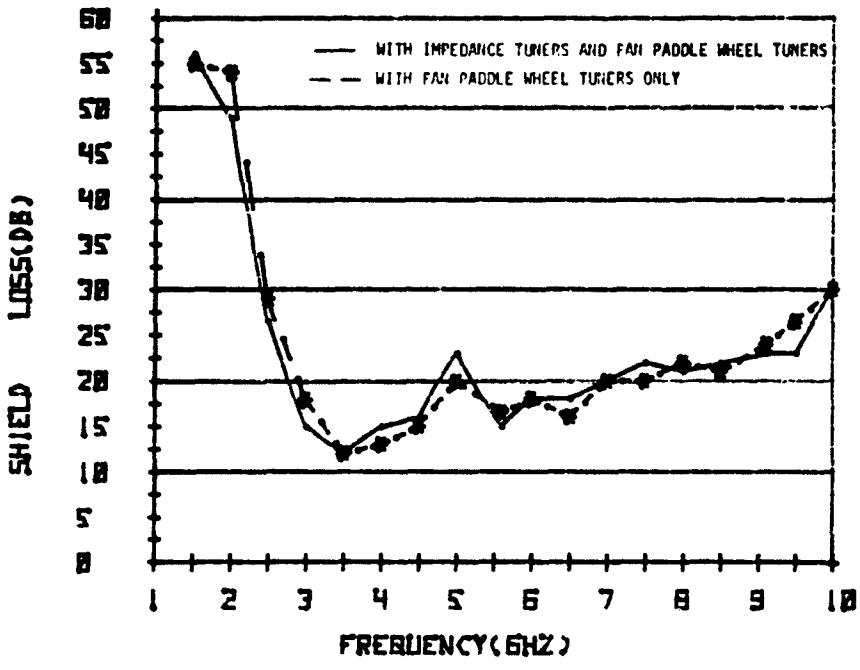

Figure A-22 Effect of Elimianting Impedance Tuners on Shield Loss of Enclosure # 5

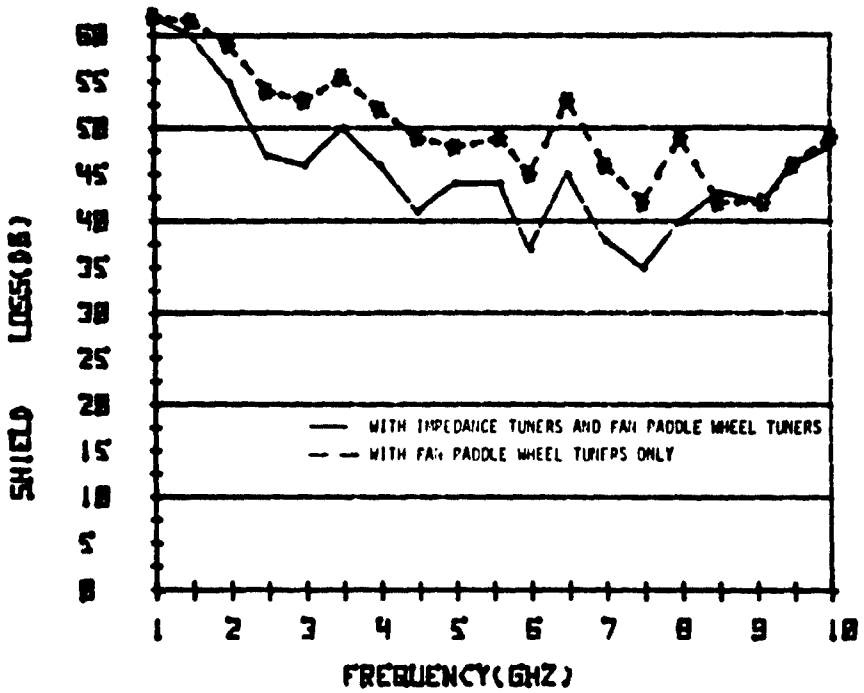

Figure A-23 Effect of Eliminating Impedance Tuners on Shield Loss of 360 Degree Shielded Twisted Pair

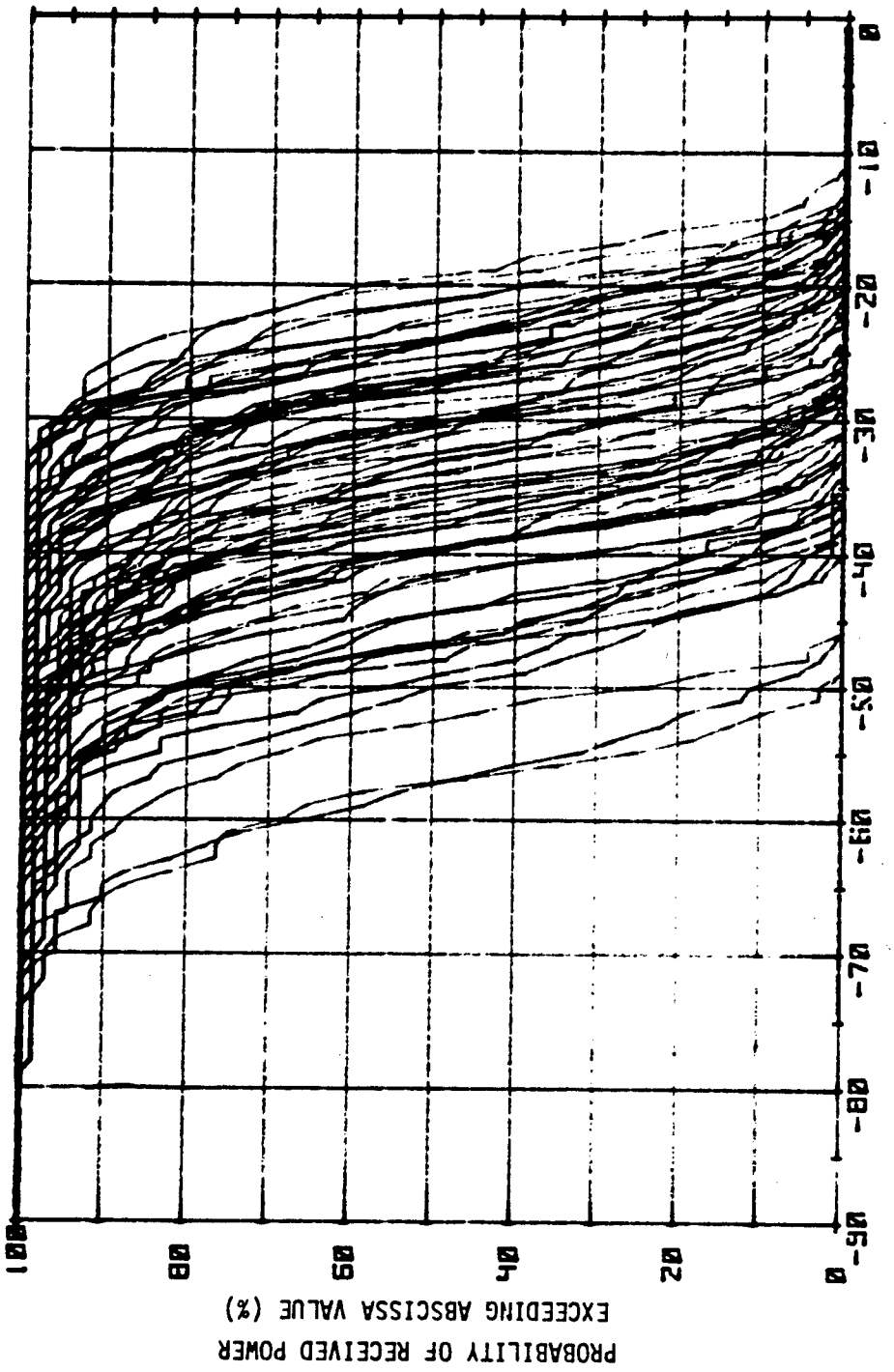

Figure A-24 Effect of Internal Paddle Wheel Tuner on Distribution of Shield Loss - Enclosure # 2 at 3 GHz

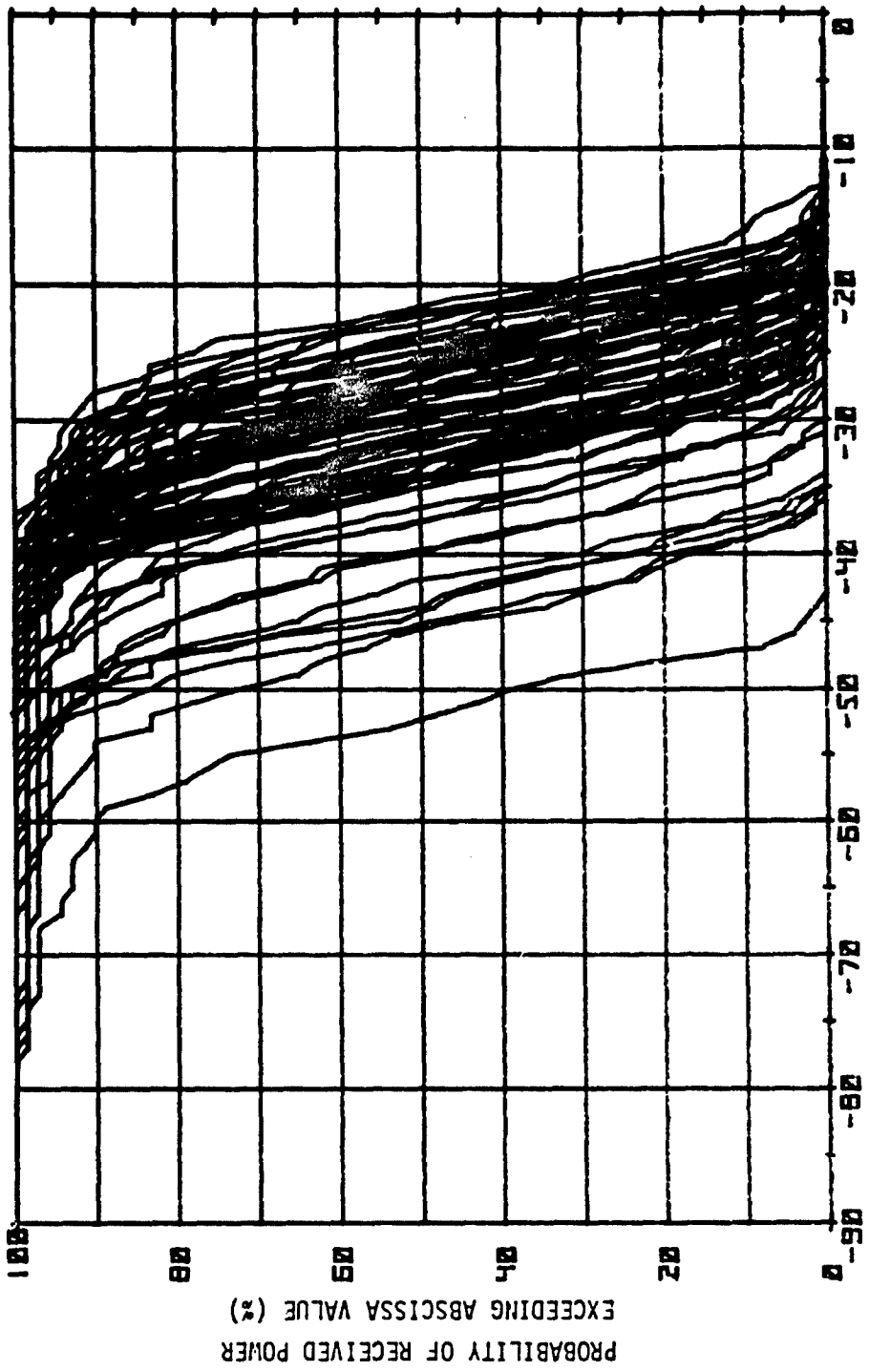

Figure A-25 Effect of Internal Paddle Wheel Tuner on Distribution of Shield Loss - Enclosure # 3 at 3 GHz

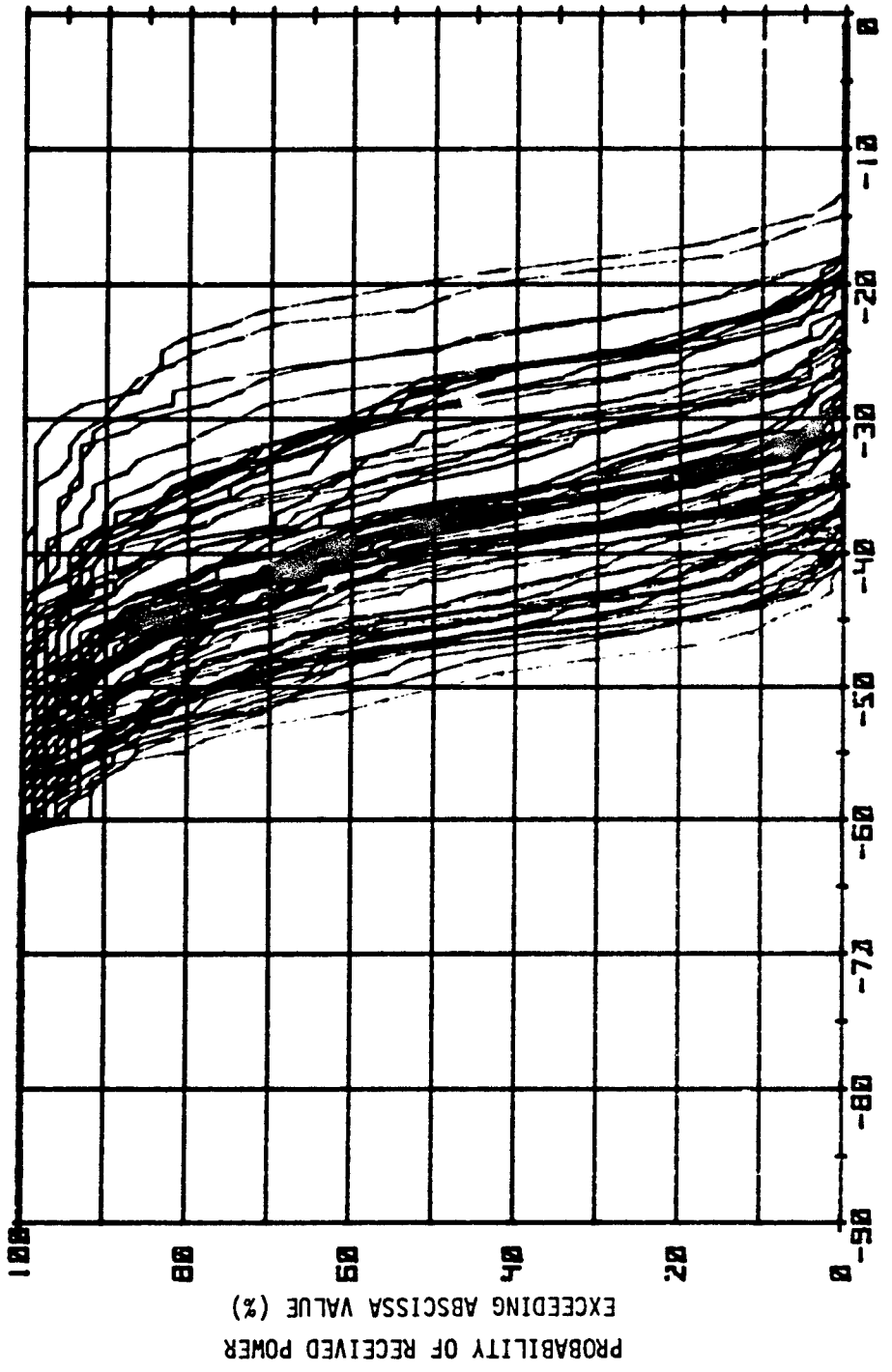

Figure A-26 Effect of Internal Paddle Wheel Tuner on Distribution of Shield Loss - Enclosure # 4 at 3 GHz

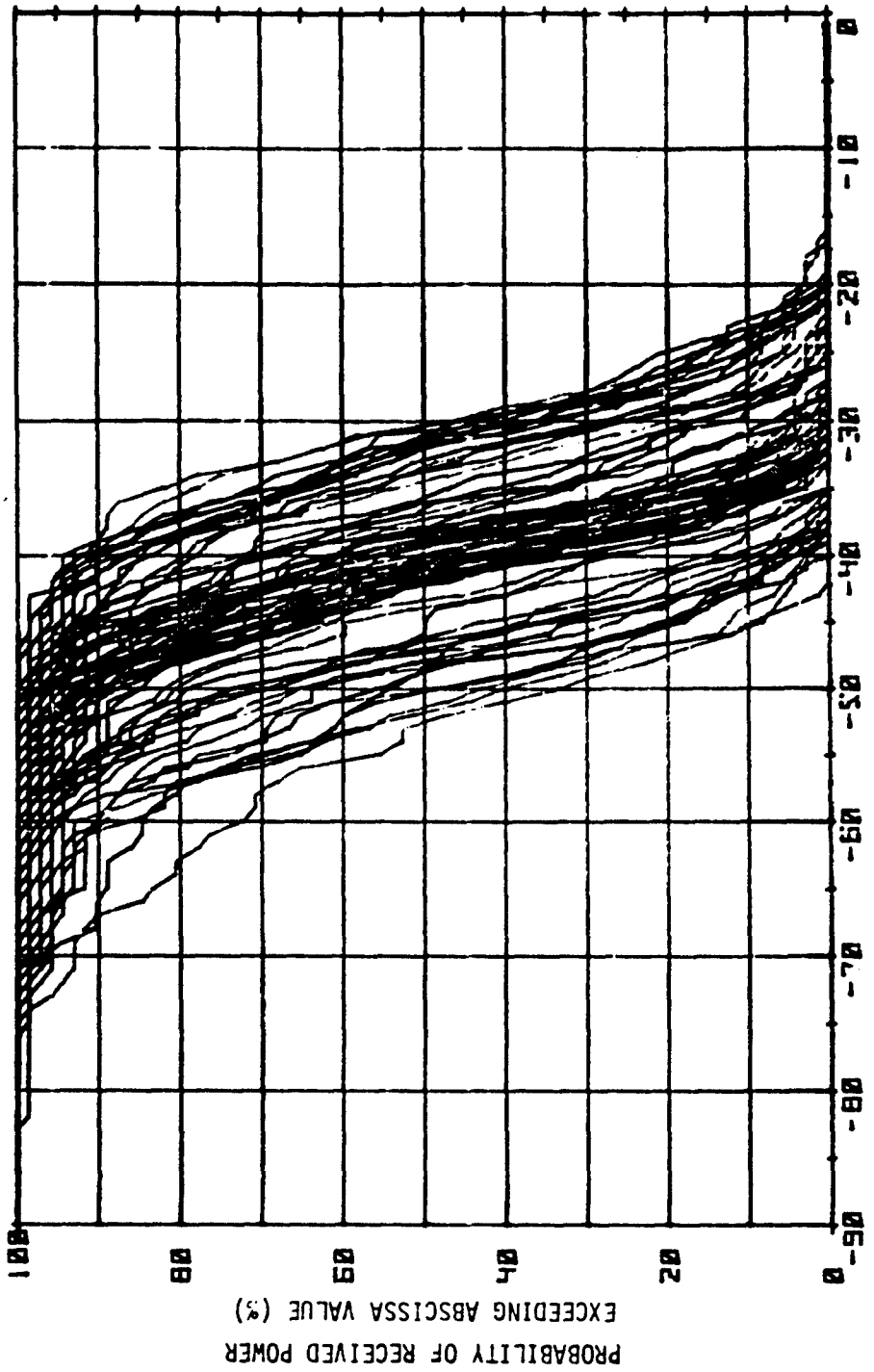

Figure A-27 Effect of Internal Paddle Wheel Tuner on Distribution of Shield Loss - Enclosure # 5 at 3 GHz

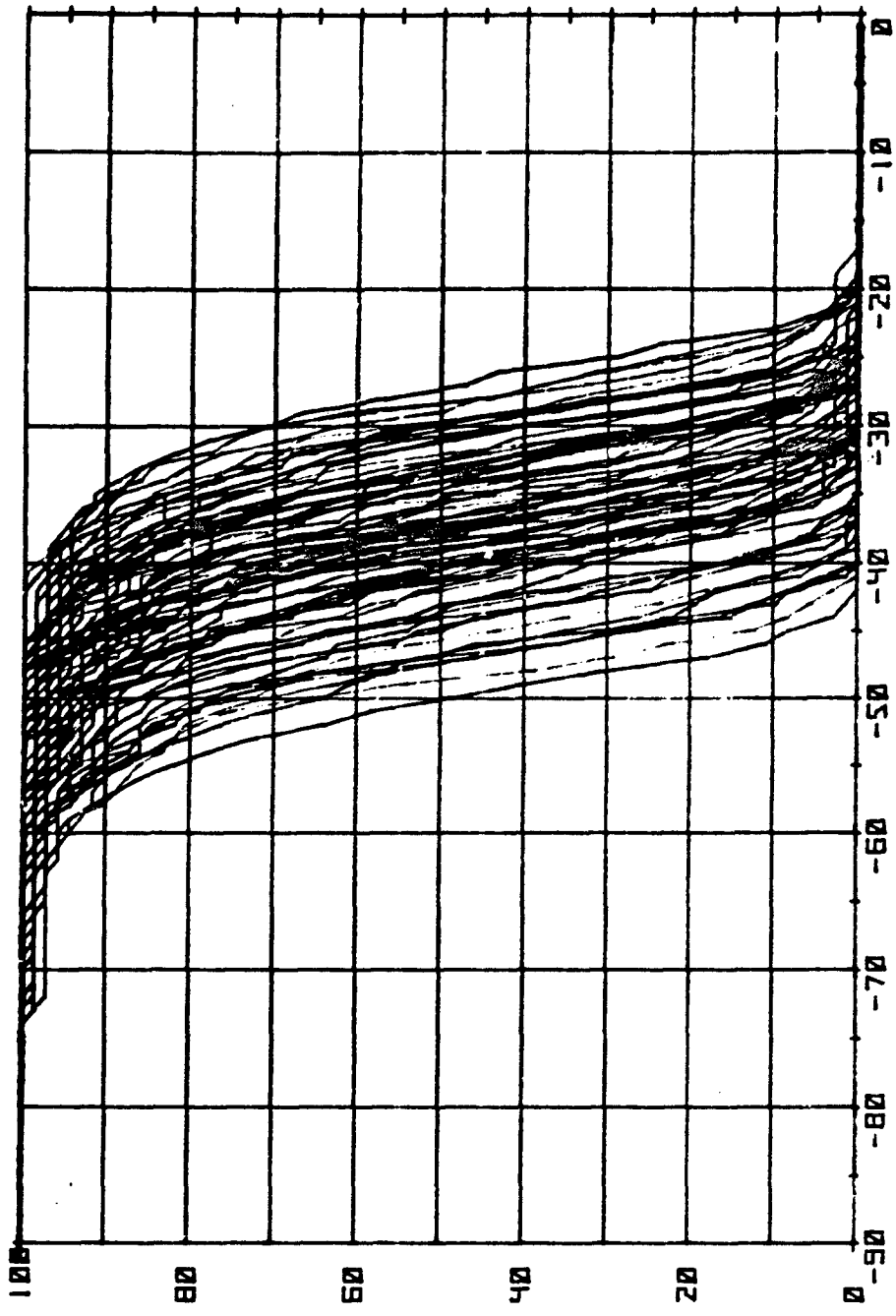

Figure A-28 Effect of Internal Paddle Wheel on Distribution of Shield Loss - Enclosure # 5 at 5.6 GHz

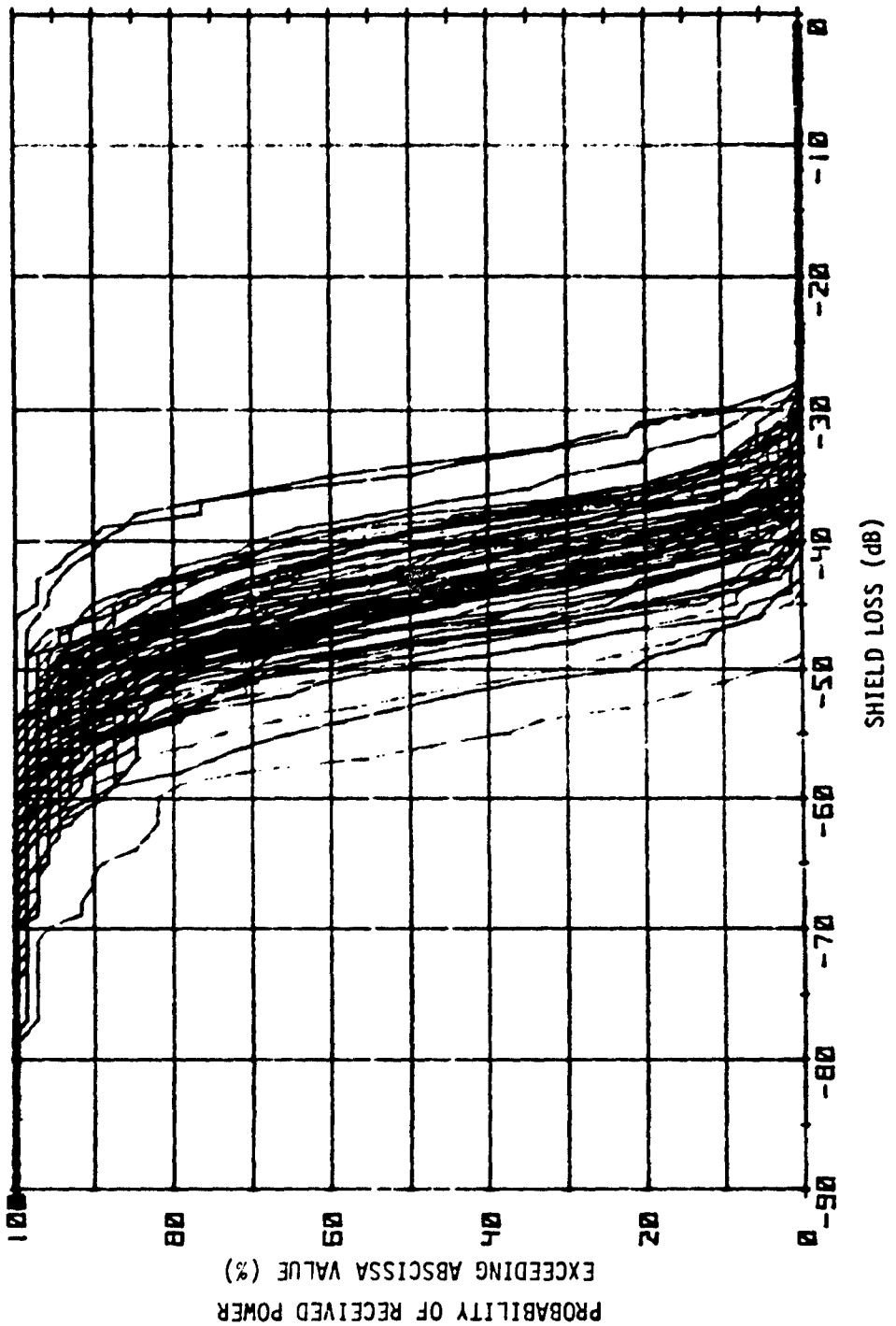

Figure A-29 Effect of Internal Paddle Wheel on Distribution of Shield Loss - Enclosure # 1 at 9.1 GHz

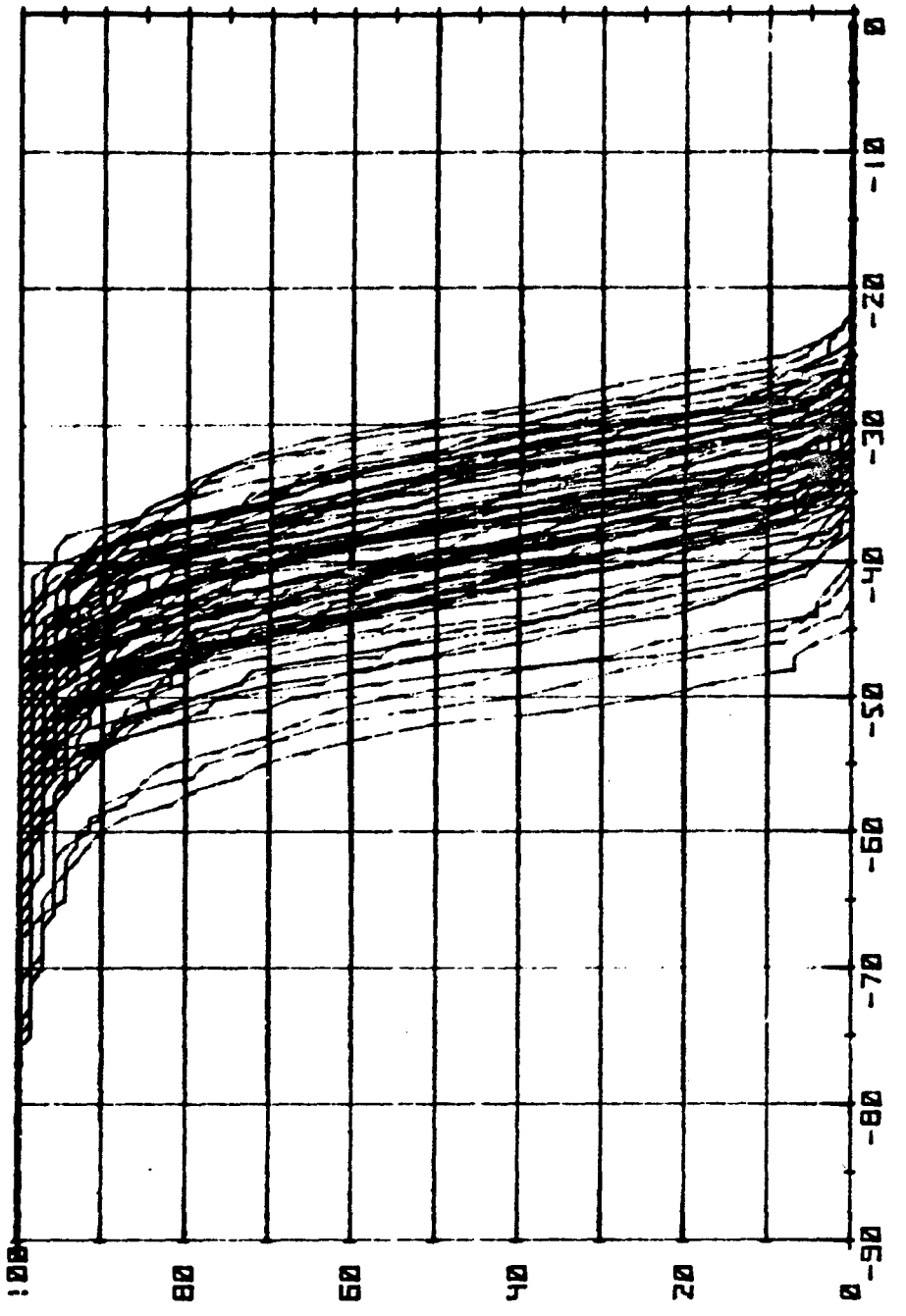

Figure A-30 Effect of Internal Paddle Wheel on Distribution of Shield Loss - Enclosure # 2 at 9.1 GHz

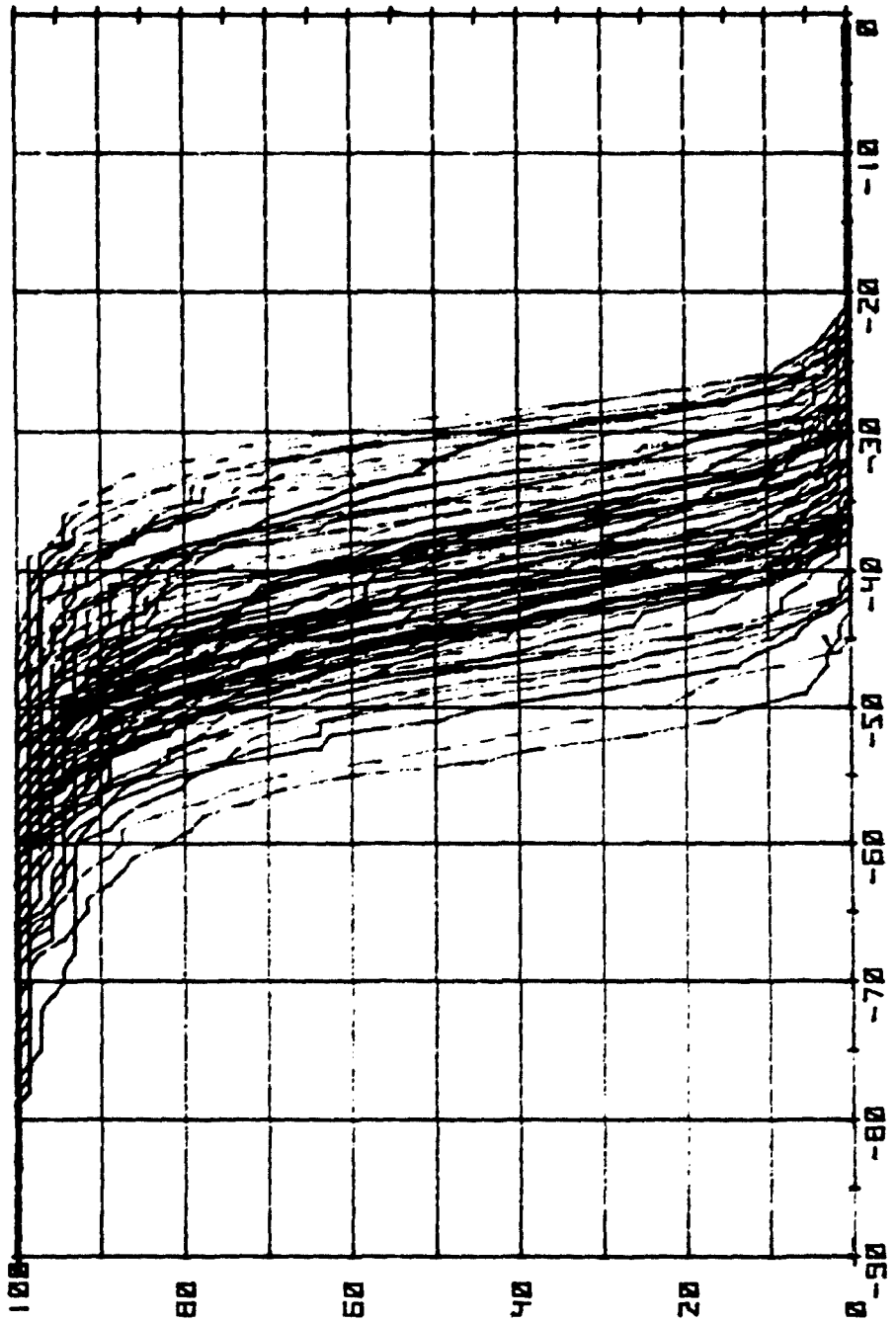

Figure A-31 Effect of Internal Paddle Wheel on Distribution of Shield Loss - Enclosure # 3 at 9.1 GHz

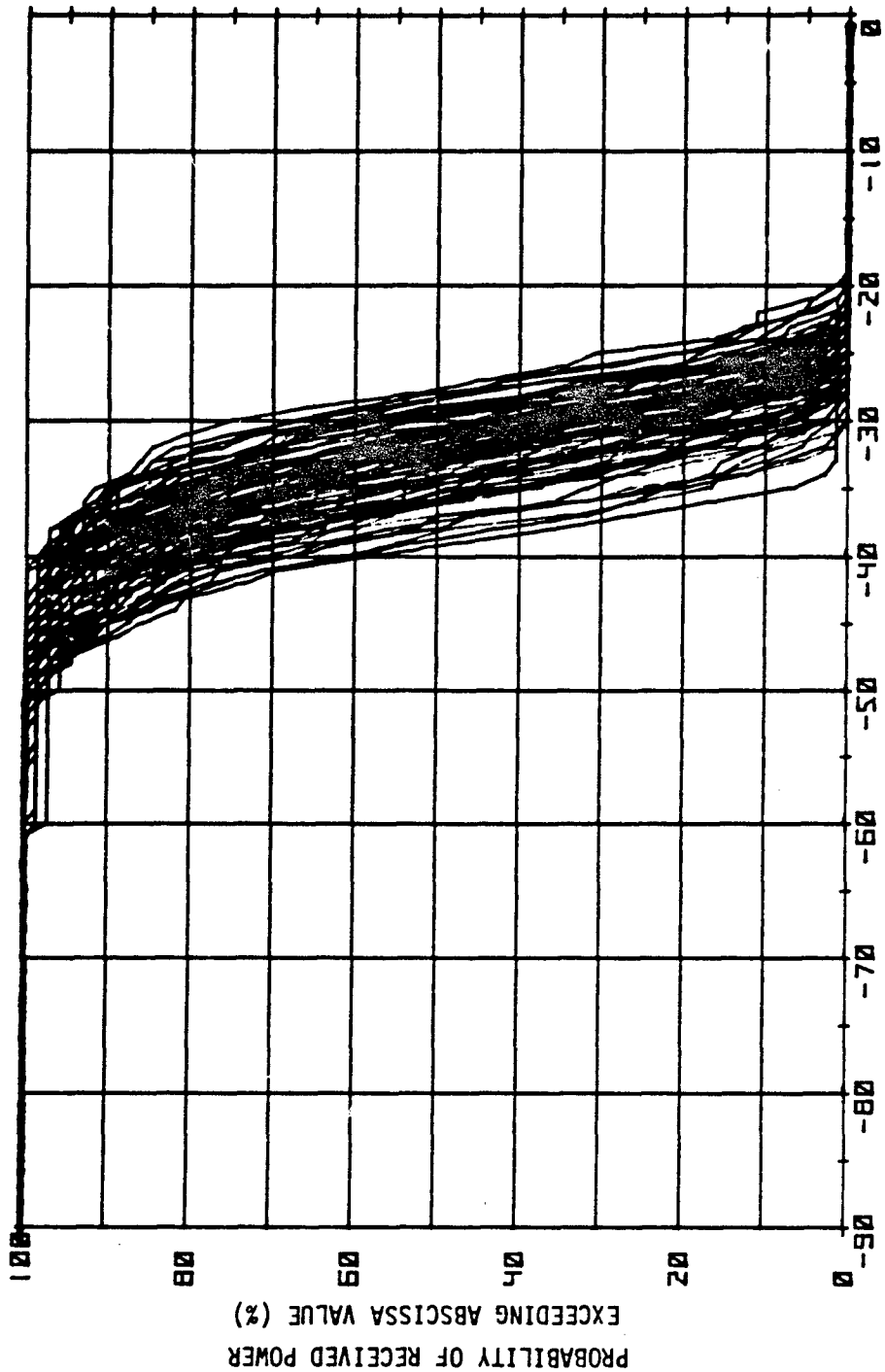

Figure A-32 Effect of Internal Paddle Wheel on Distribution of Shield Loss - Enclosure # 4 at 9.1 GHz

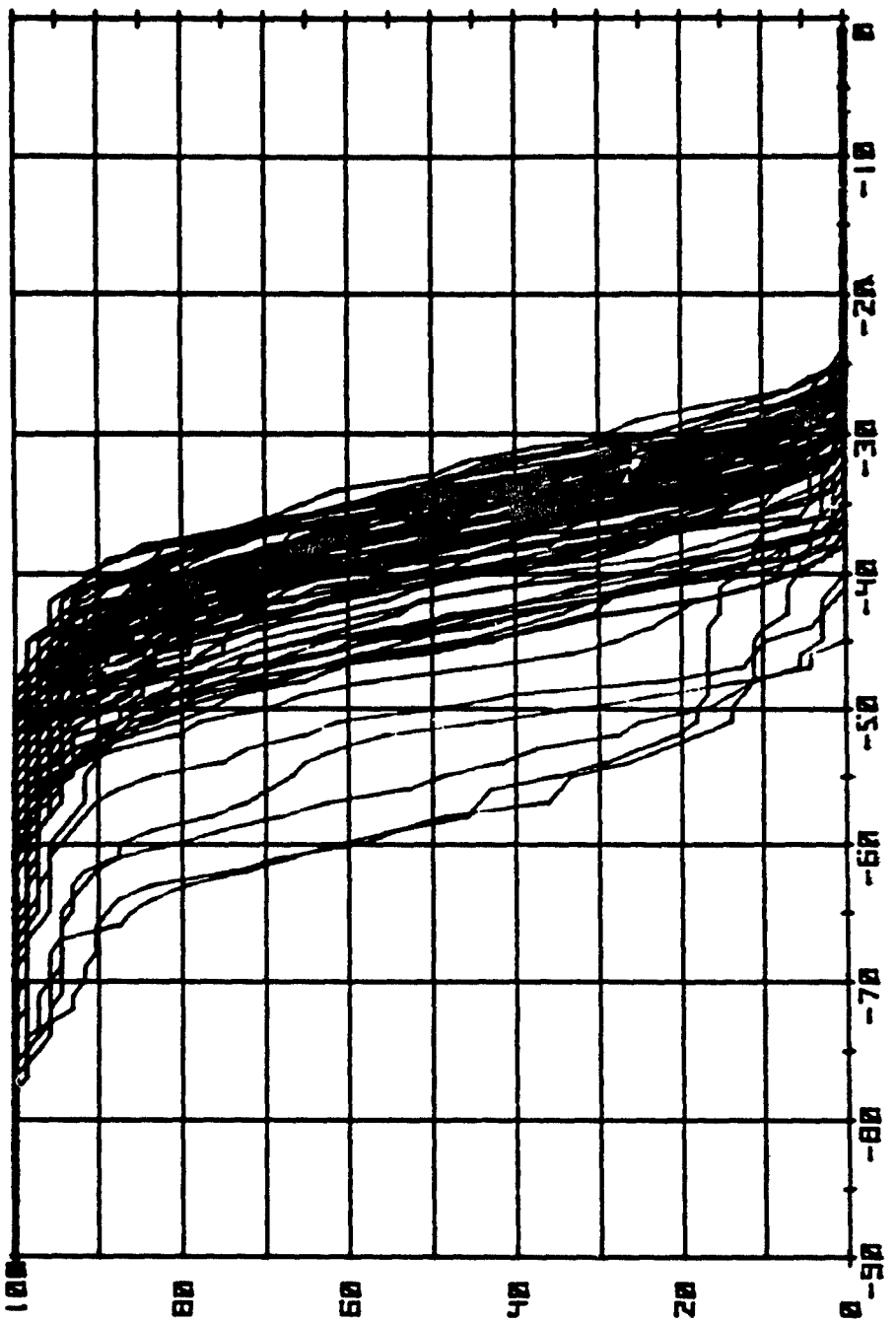

Figure A-33 Effect of Internal Paddle Wheel on Distribution of Shield Loss - Enclosure # 5 at 9.1 GHz

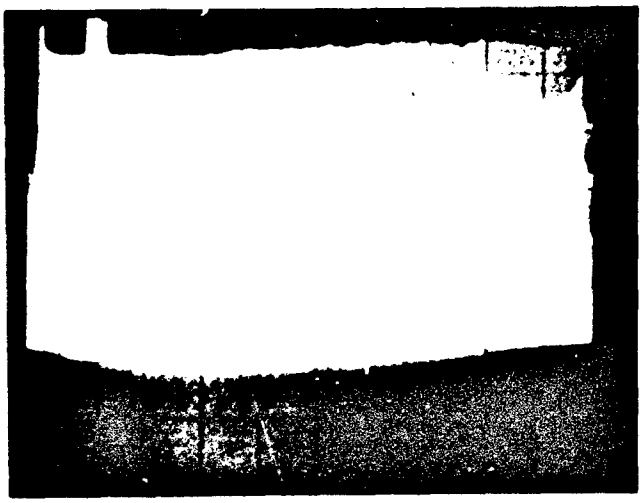

a) Reference Signal

b) Calibration Signal

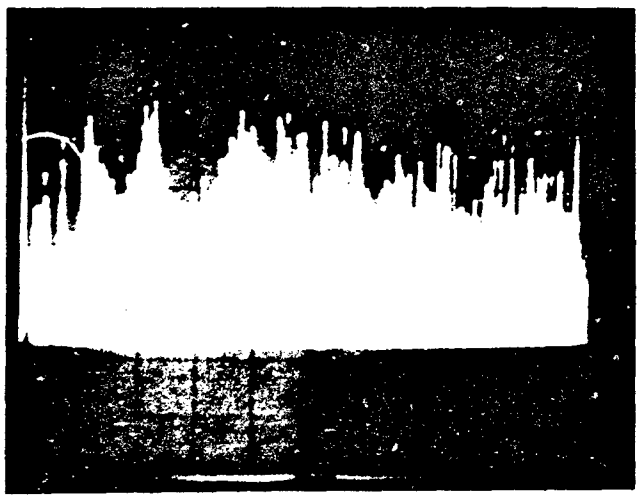

c) Shield Loss Signal

Figure A-34

Swept Frequency Measurement of
Enclosure # 1 Shielding Effectiveness

Vertical = 10 dB/div.
Horizontal = 200 MHz/div.

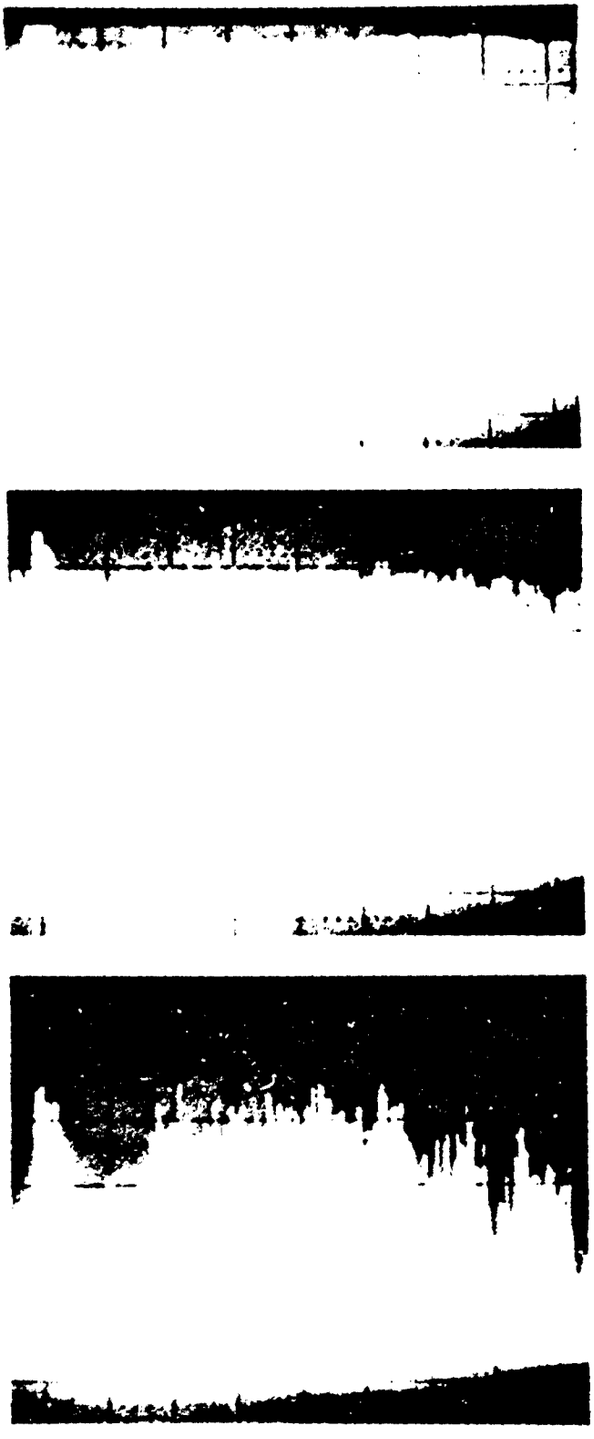

a) Reference Signal

b) Calibration Signal

c) Shield Loss Signal

Figure A-35
Swept Frequency Measurement of
Enclosure # 2 Shielding Effectiveness

Vertical = 10 dB/div.
Horizontal = 200 MHz/div.

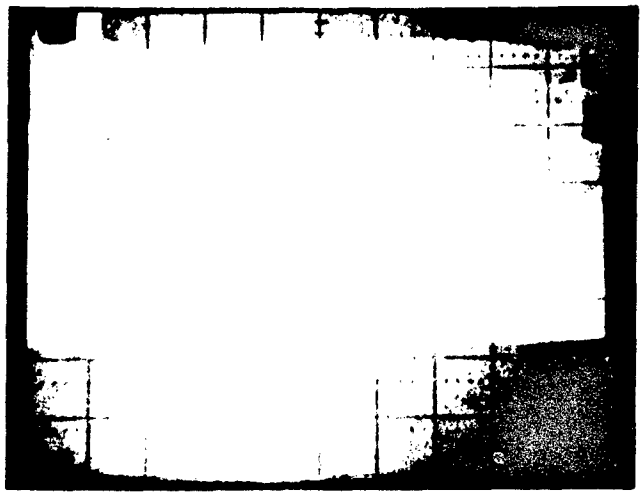

a) Reference Signal

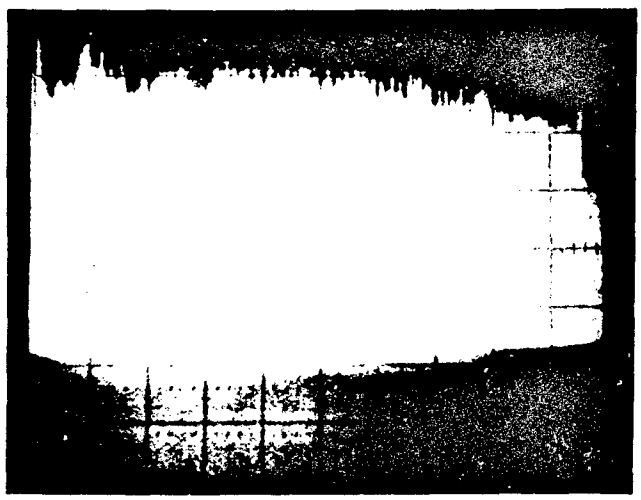

b) Calibration Signal

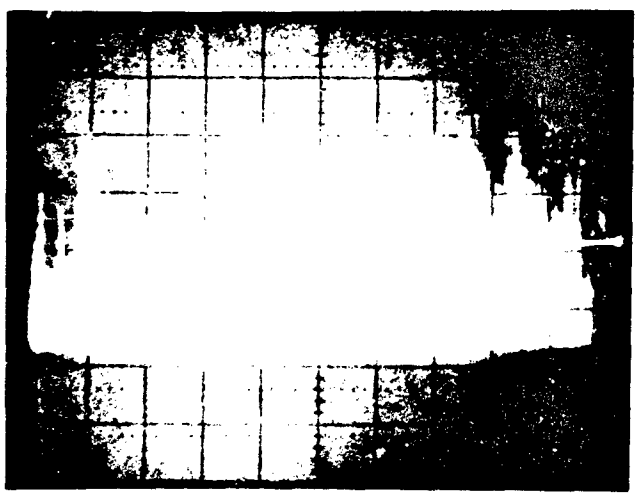

c) Shield Loss Signal

Figure A-36
Swept Frequency Measurement of
Enclosure # 3 Shielding Effectiveness

Vertical = 10 dB/div.
Horizontal = 200 MHz/div.

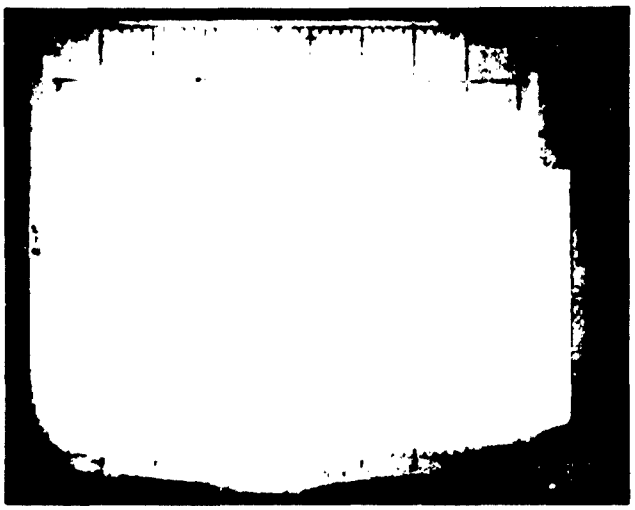

3) Reference Signal

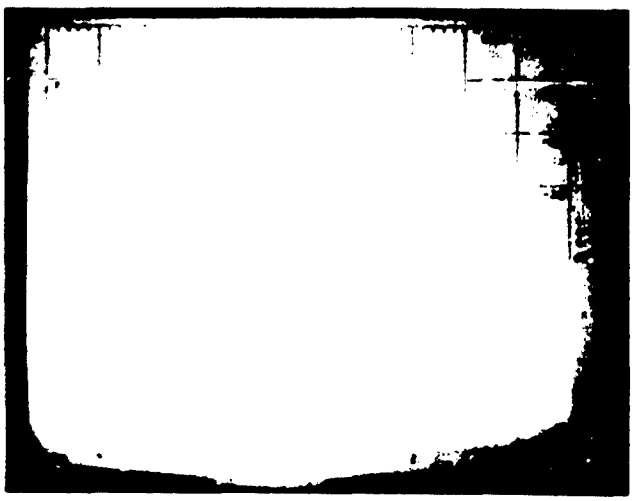

b) Calibration Signal

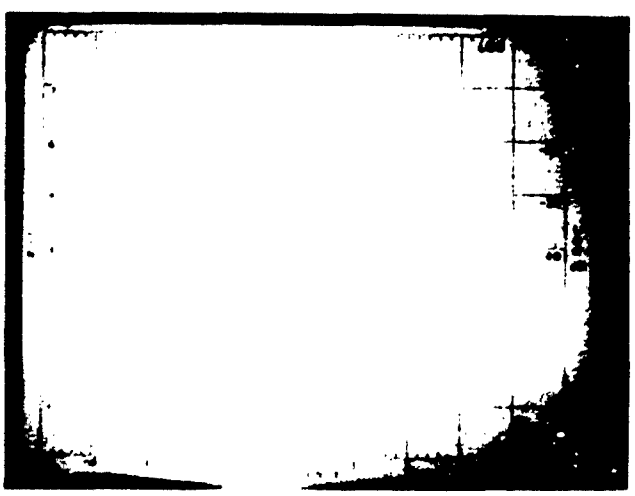

c) Shield Loss Signal

Figure A-37
Swept Frequency Measurement of
Enclosure # 4 Shielding Effectiveness

Vertical = 10 dB/div.
Horizontal = 200 MHz/div.

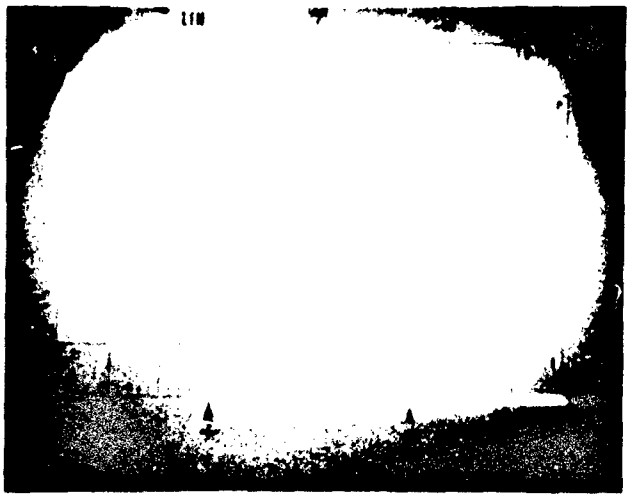

3) Reference Signal

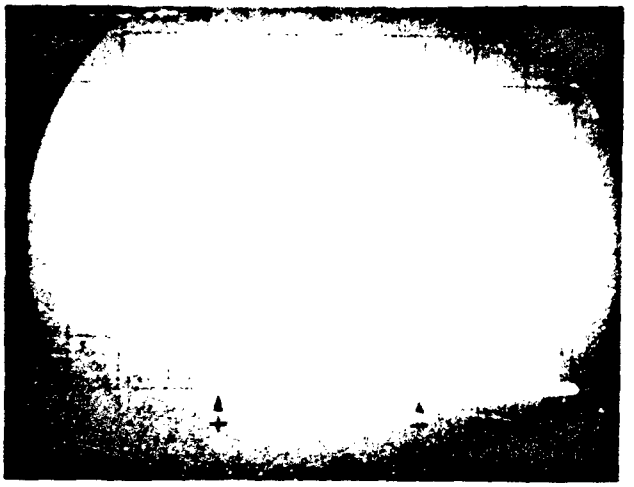

b) Calibration Signal

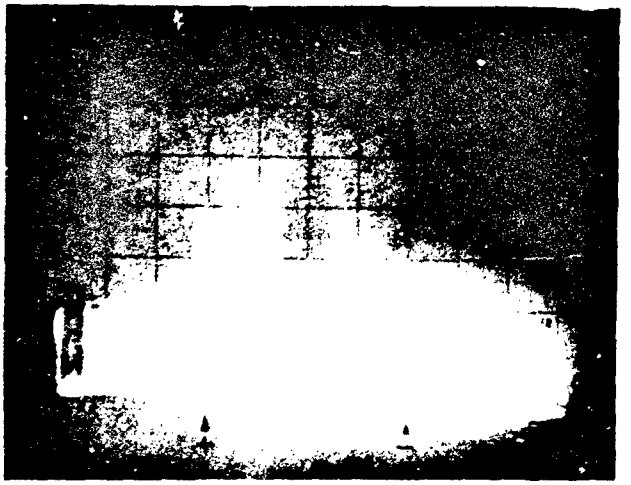

c) Shield Loss Signal

Figure A-38
Swept Frequency Measurements of
360° Shielded Twisted Pair

Vertical = 10 dB/div.
Horizontal = 200 MHz/div.

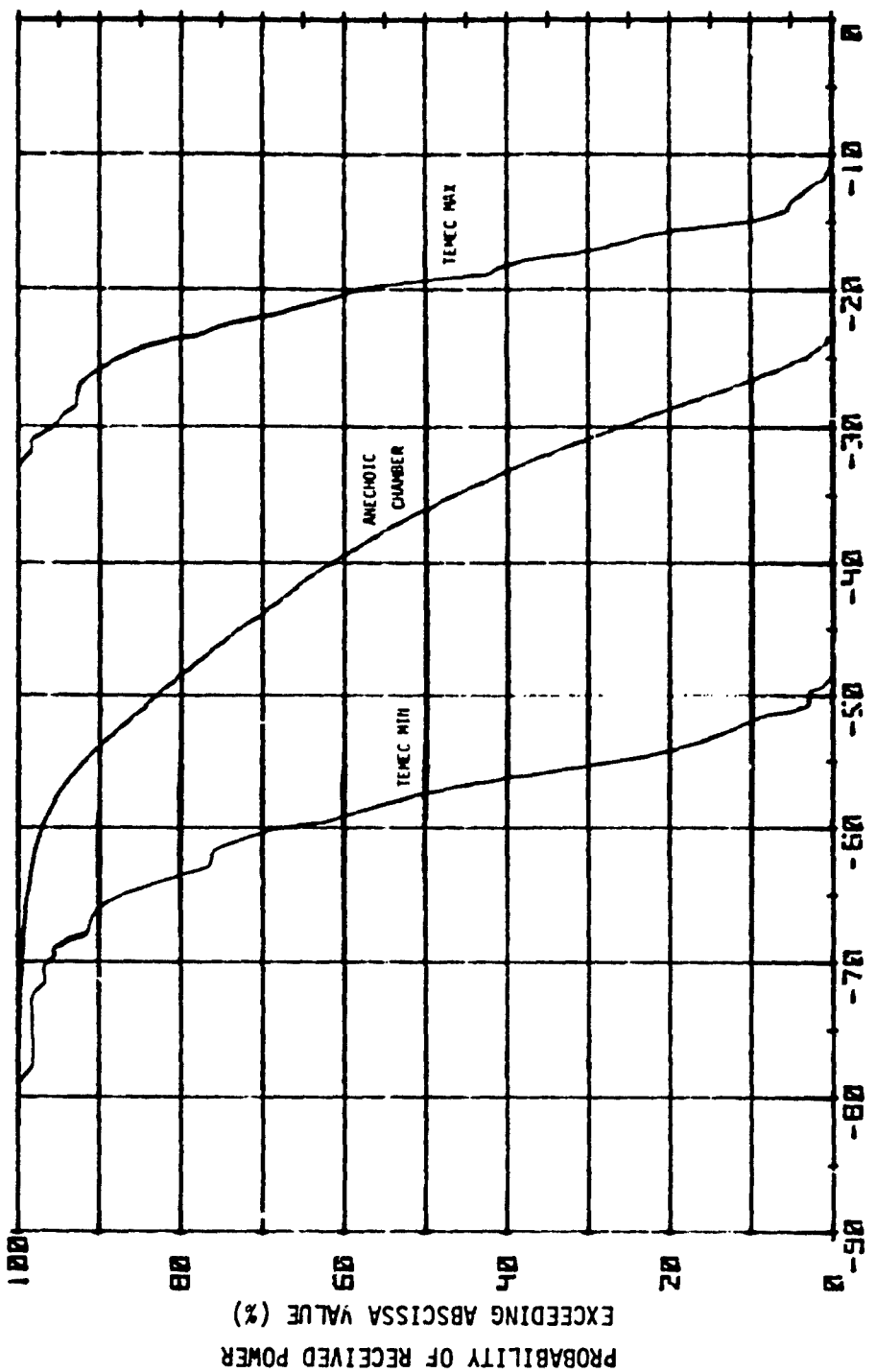

Figure A-39 Comparison of TEMEC to Anechoic Chamber Measurement of Distribution of Received Power - Enclosure # 2 at 3 GHz in 1 W/M^2 Field

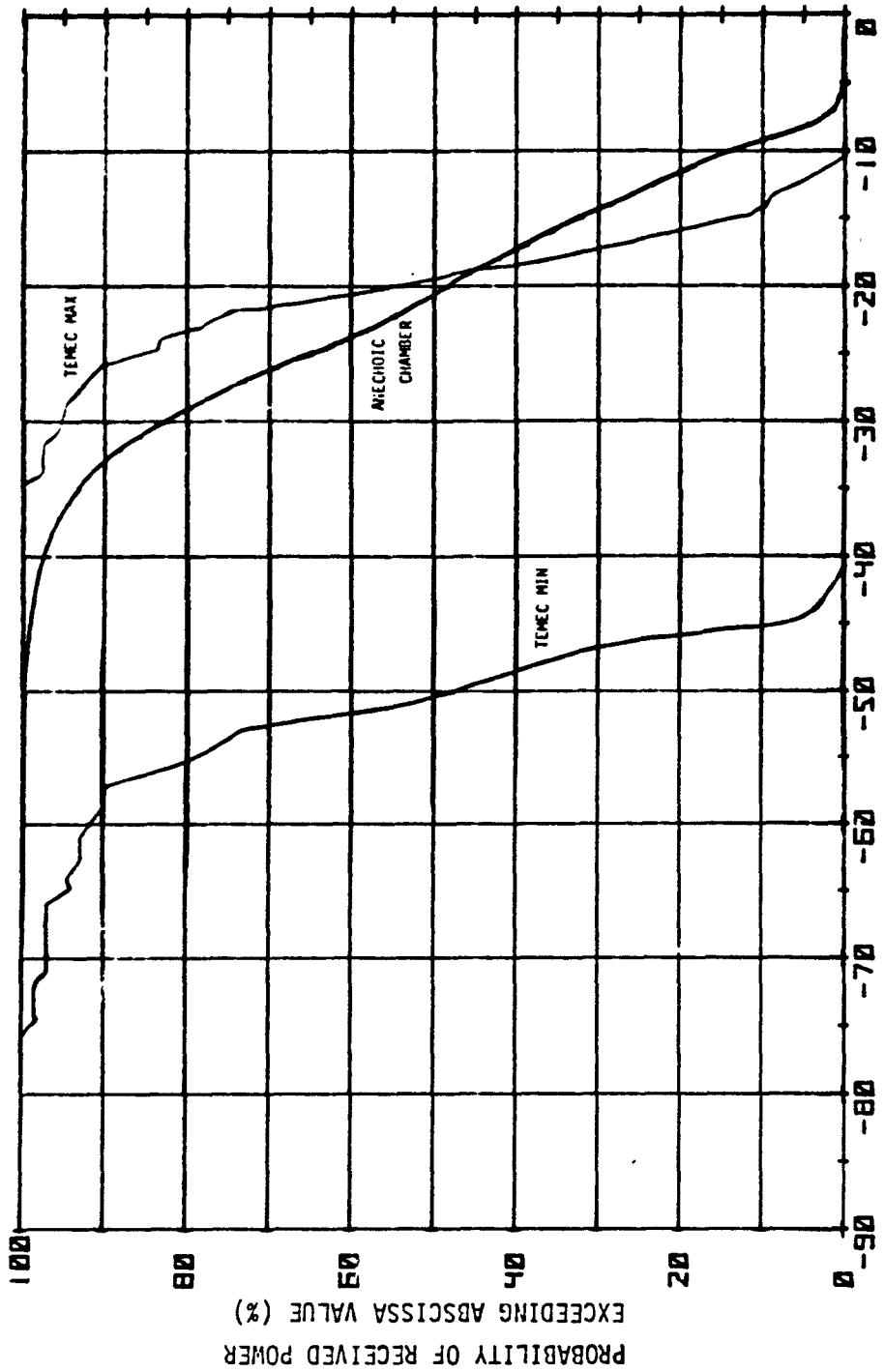

Figure A-40 Comparison of TEMEC to Anechoic Chamber Measurement of Distribution of Received Power - Enclosure # 3 at 3 GHz in 1 W/M^2 Field

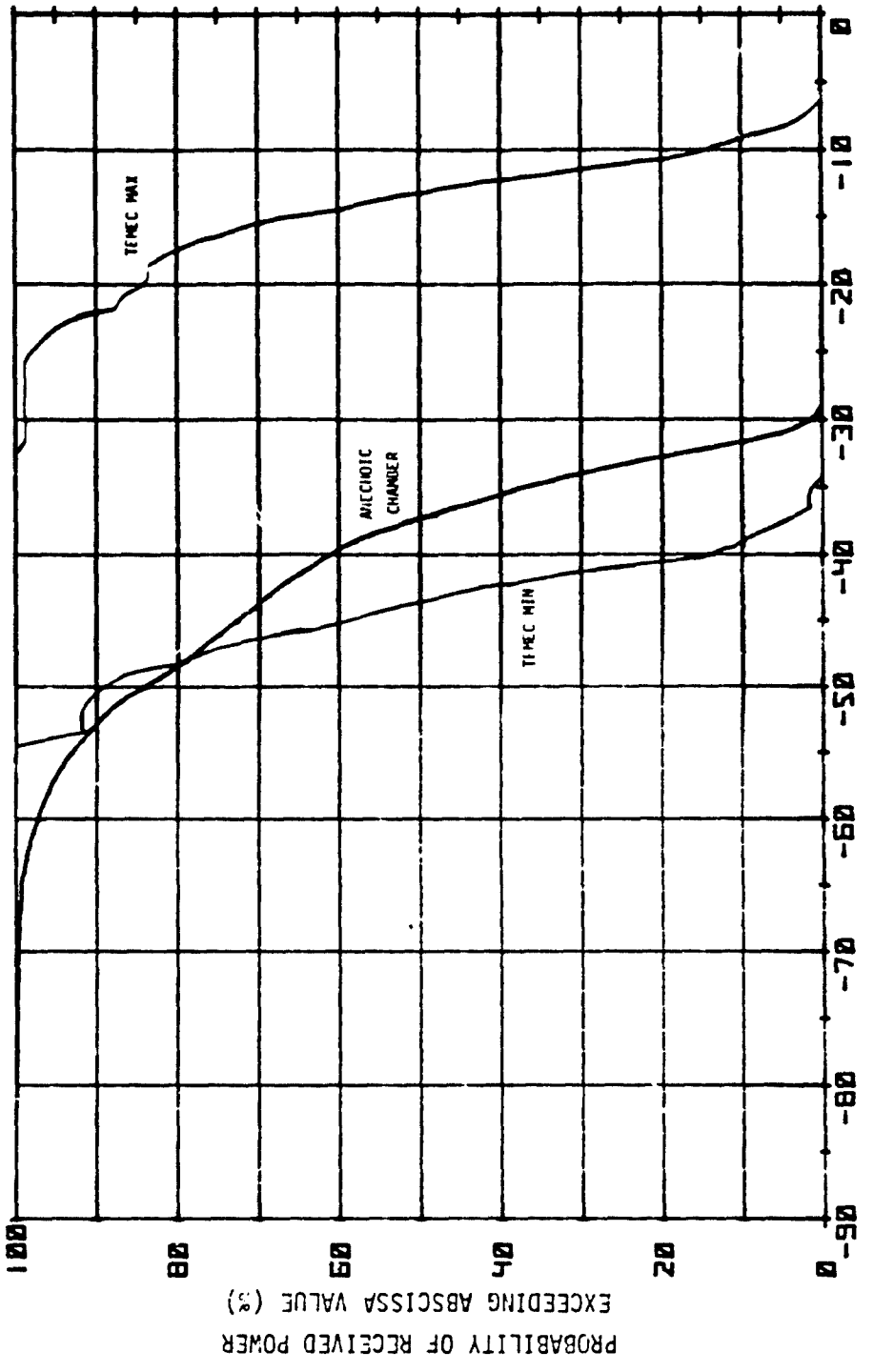

Figure A-41 Comparison of TEMEC to Anechoic Chamber Measurement of Distribution of Received Power - Enclosure # 4 at 3 GHz in 1 W/M^2 Field

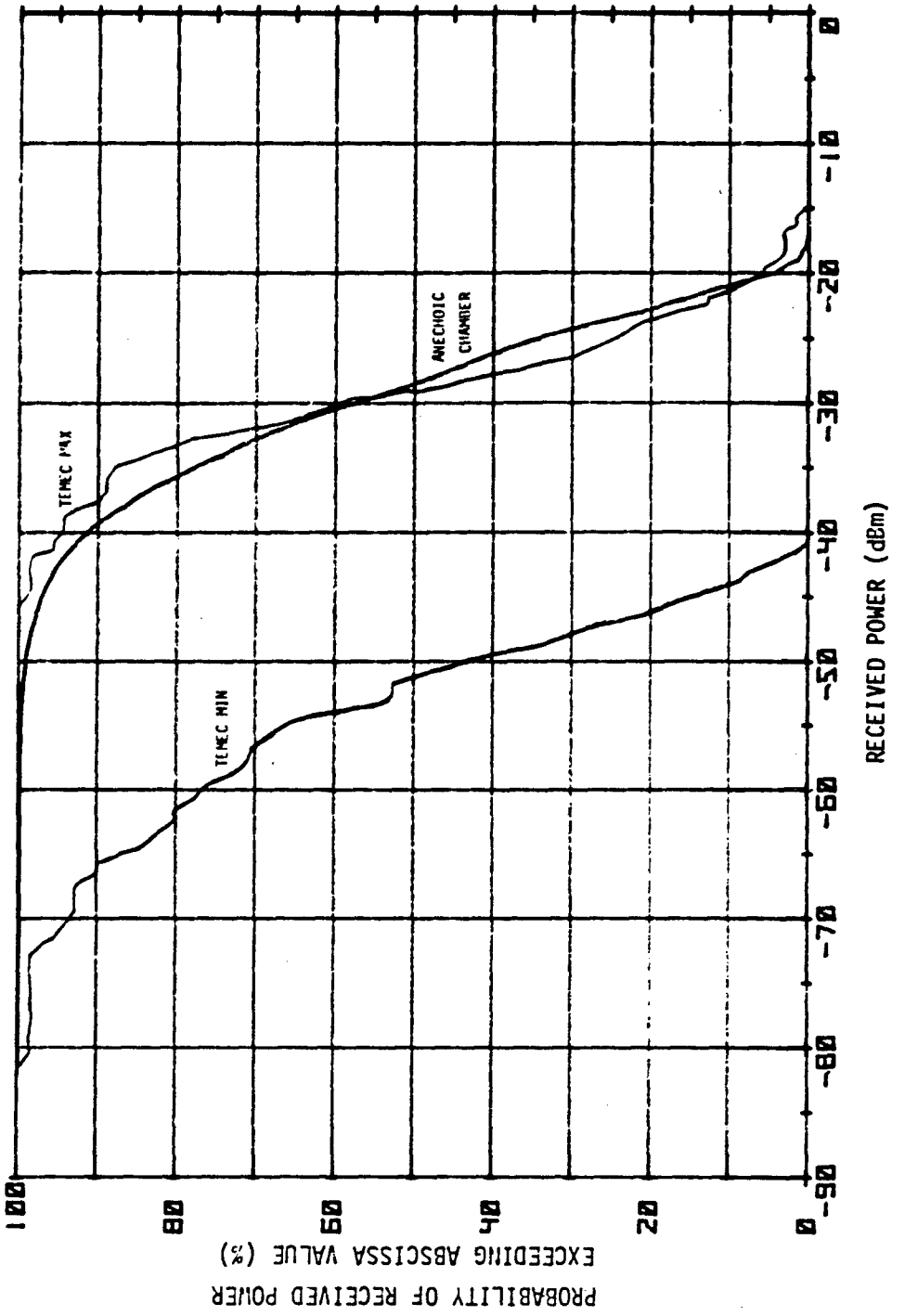

Figure A-42 Comparison of TEMEC to Anechoic Chamber Measurement of Distribution of Received Power - Enclosure # 5 at 3 GHz in 1 W/M^2 Field

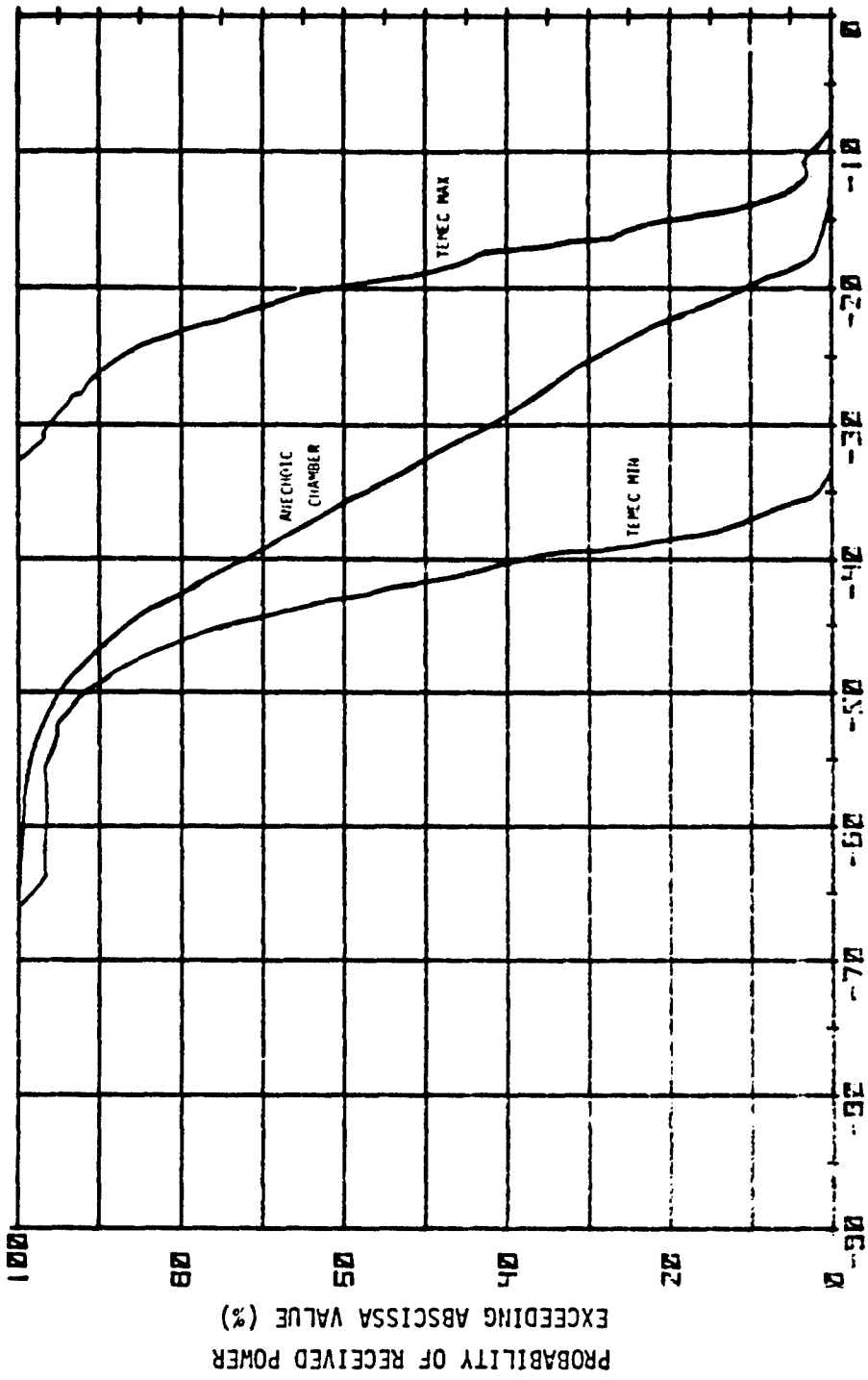

Figure A-43 Comparison of TEMEC to Anechoic Chamber Measurement of Distribution of Received Power - Enclosure # 5 at 5.6 GHz in 1 W/M^2 Field

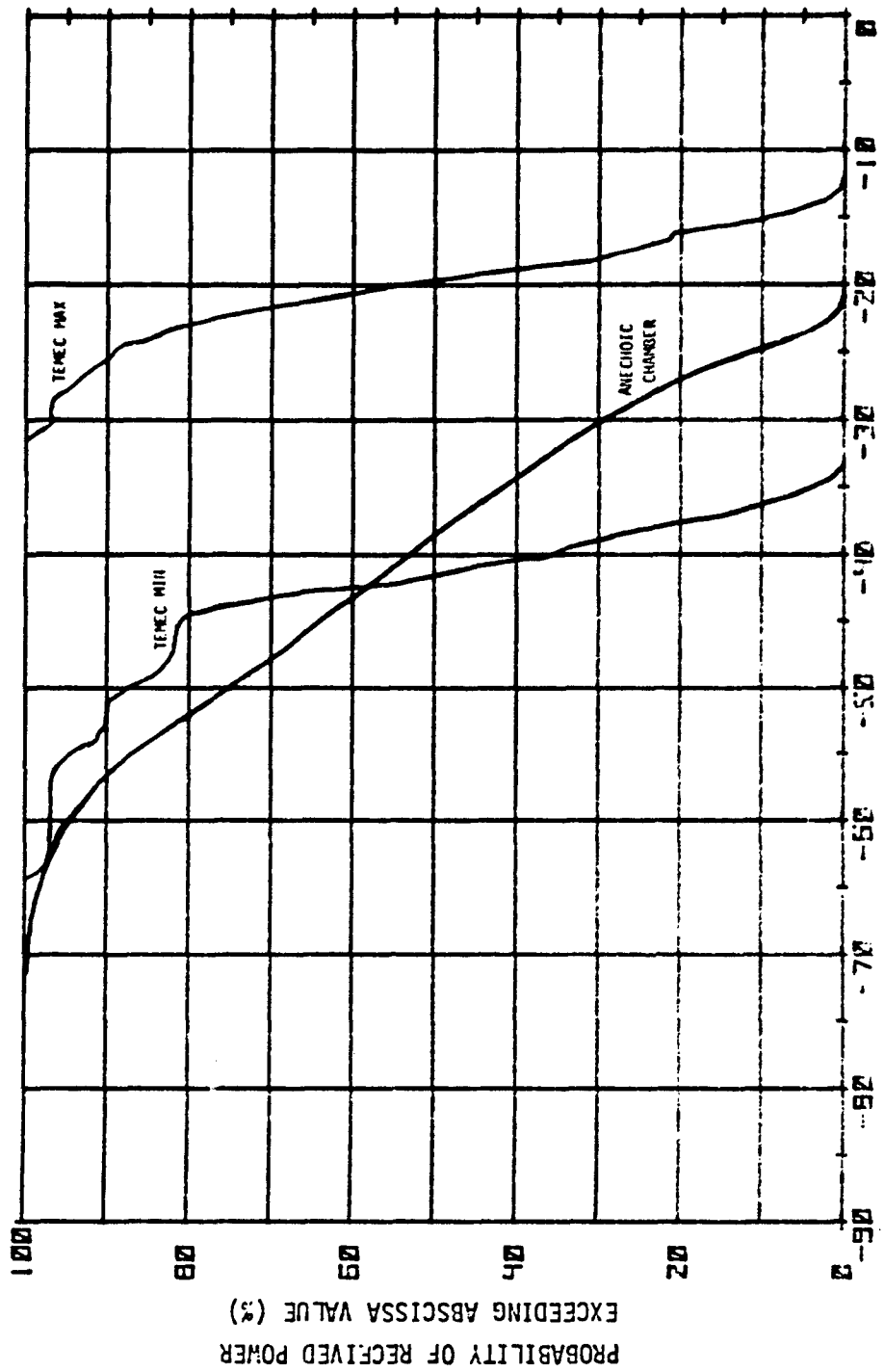

Figure A-44 Comparison of TEMEC to Anechoic Chamber Measurement of Distribution of Received Power - Enclosure # 1 at 9.1 GHz in 1 W/M^2 Field

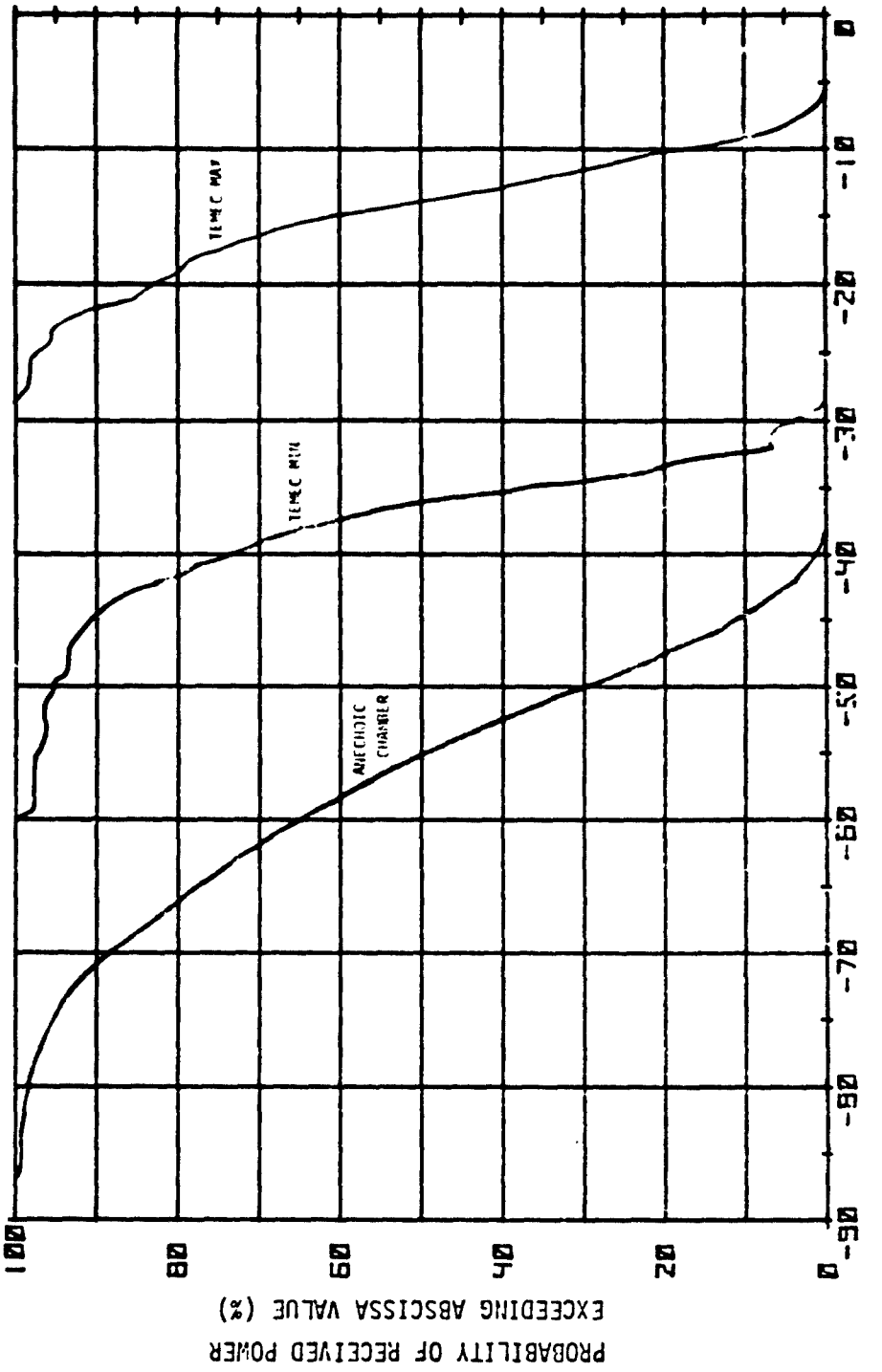

Figure A-45 Comparison of TEMEC to Anechoic Chamber Measurement of Distribution of Received Power - Enclosure # 2 at 9.1 GHz in 1 W/M^2 Field

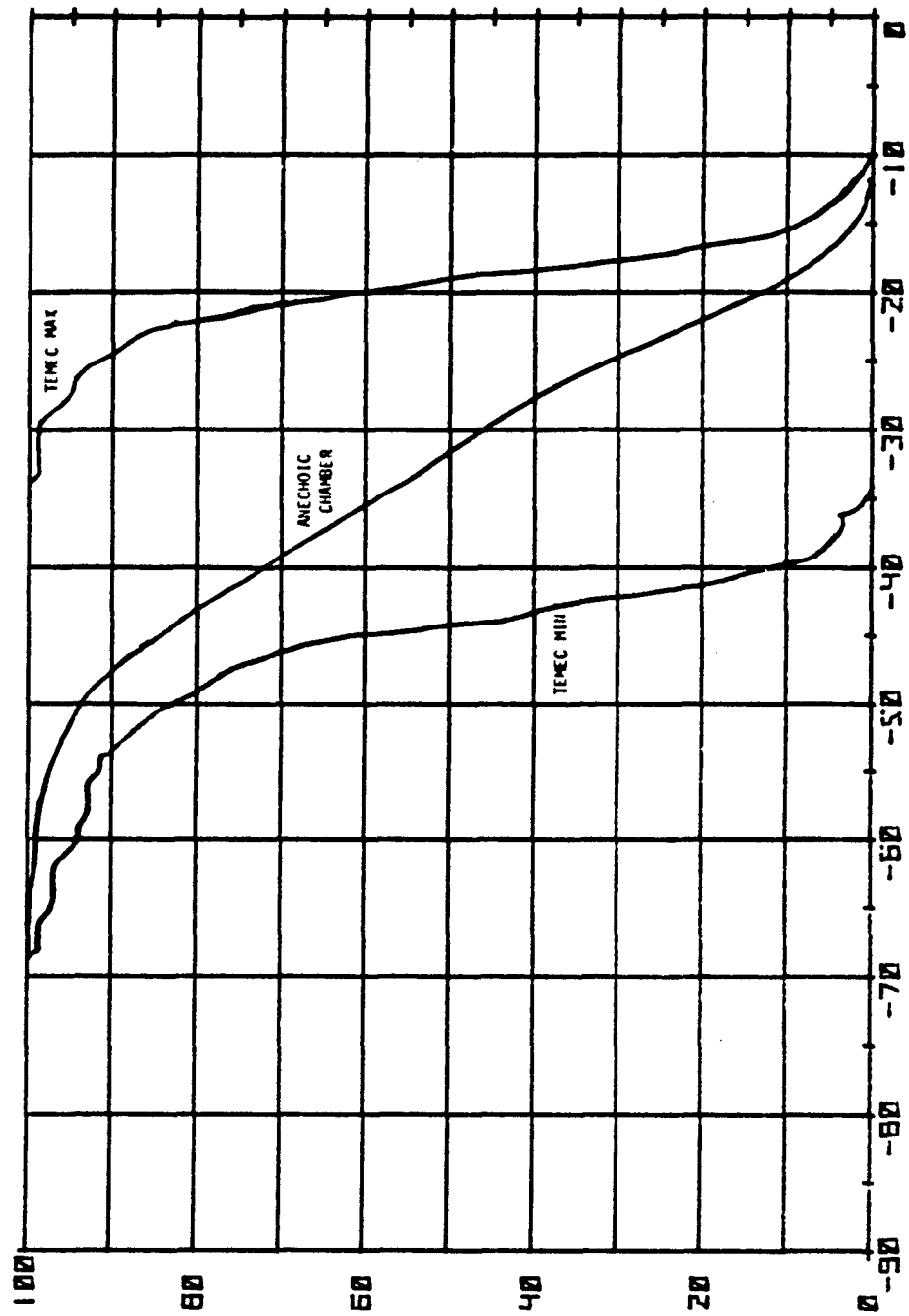

Figure A-46 Comparison of TEMEC to Anechoic Chamber Measurement of Distribution of Received Power - Enclosure # 3 at 9.1 GHz in 1 W/M^2 Field

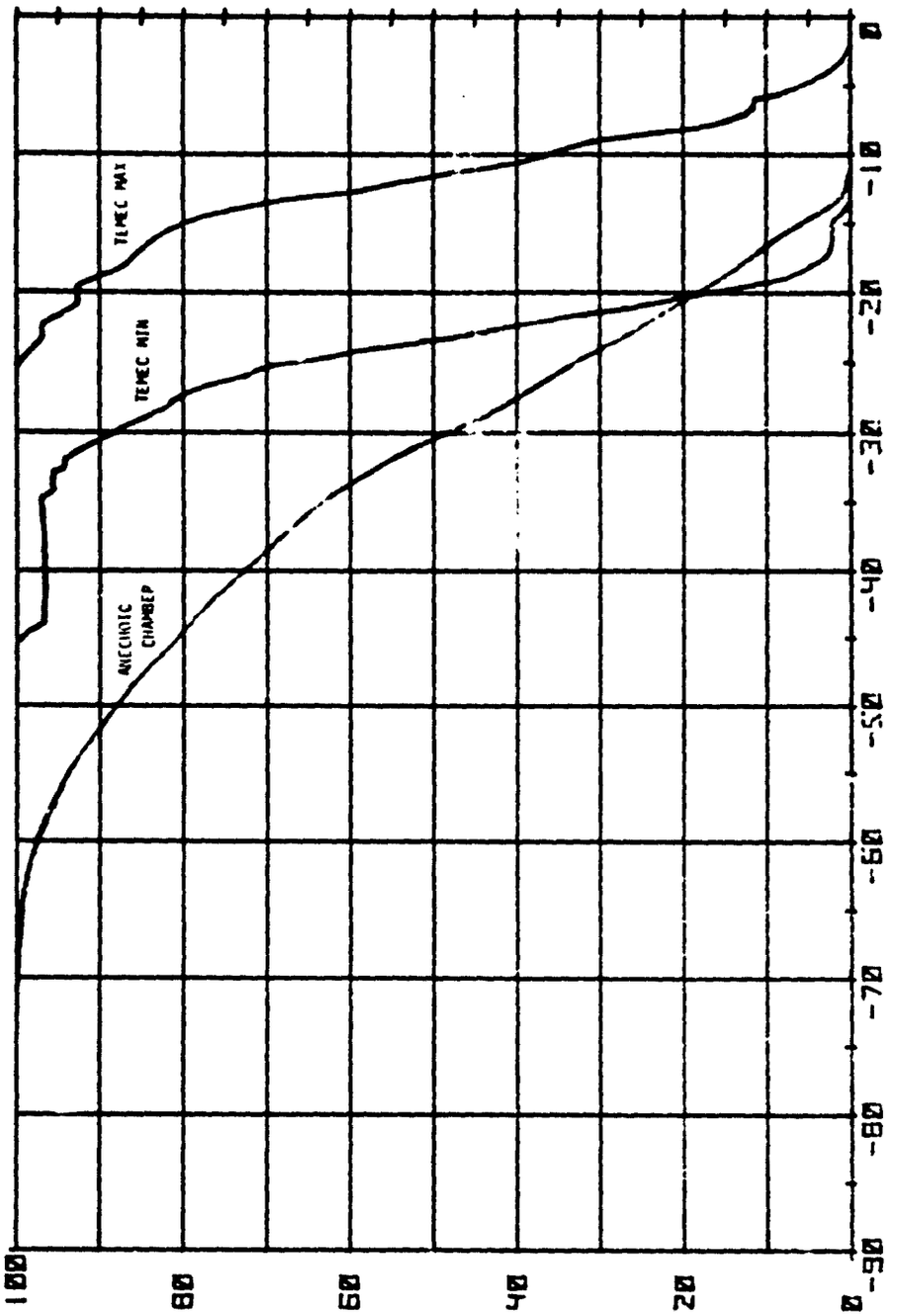

Figure A-47 Comparison of TEMEC to Anechoic Chamber Measurement of Distribution of Received Power - Enclosure # 4 at 9.1 GHz in 1 W/M^2 Field

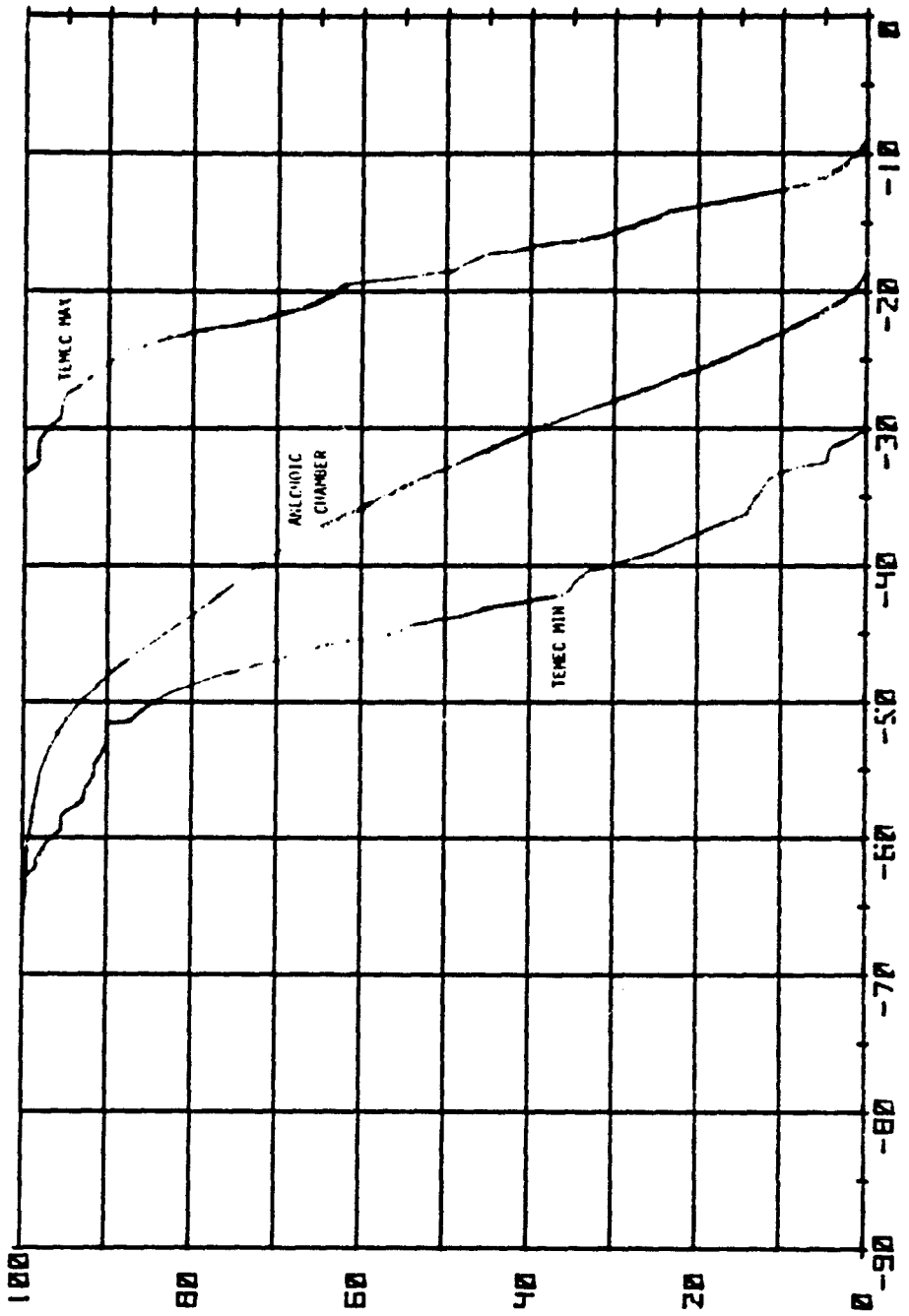

Figure A-48 Comparison of TEMEC to Anechoic Chamber Measurement of Distribution of Received Power - Enclosure # 5 at 9.1 GHz in 1 W/M^2 Field